Engineering Structures 254 (2022) 113860

Contents lists available at ScienceDirect

Engineering Structures

journal homepage: www.elsevier.com/locate/engstruct

Critical analysis on the use of the shove test for investigating the shear-sliding behavior of brick masonry

Francesca Ferretti [a,*], Samira Jafari [b], Rita Esposito [b], Jan G. Rots [b], Claudio Mazzotti [a]

[a] Department of Civil, Chemical, Environmental and Materials Engineering, University of Bologna, Viale Risorgimento 2, 40136 Bologna, Italy
[b] Faculty of Civil Engineering and Geosciences, Delft University of Technology, Stevinweg 1, 2628 CN Delft, The Netherlands

ARTICLE INFO

Keywords:
Unreinforced brick masonry
Shear-sliding behavior
Shove test
Brick-to-brick model
Nonlinear analyses

ABSTRACT

The shove test (ASTM Standard C1531) is an experimental technique aimed at studying the shear-sliding behavior of brick masonry. It can be executed according to various testing methods that differ in the way the vertical compression load is applied and in the way bricks and/or joints are locally removed for inserting jacks. One of the most critical aspects is the correct evaluation of the compressive stress state on the sliding brick. The objective of the present paper is to investigate the capability of the shove test in determining the shear strength parameters of brick masonries and to highlight the main advantages and disadvantages of the various testing methods. To this aim, nonlinear numerical simulations of the shove test were performed by adopting a brick-to-brick modeling strategy. The 2D numerical model was calibrated and validated through comparisons with experimental results of triplet tests and shove tests. The numerical analyses allowed to understand the influence the different testing methods and the masonry mechanical properties, such as dilatancy, may have on the test results. Based on the numerical outcomes, correction factors were calibrated for the proper evaluation of the compressive stress state on the sliding brick. Improvements with regards to the experimental procedures, i.e. additional test phases and measurements, were also proposed to enhance the results interpretation.

1. Introduction

In a masonry panel subject to lateral in-plane loading, the possible failure modes are typically associated to three different mechanisms: rocking, diagonal cracking or sliding [1–5]. The activation of a sliding mechanism, which is the failure mode investigated in this paper, could take place either along a horizontal crack in a bed joint or in presence of a stair-stepped diagonal crack, as also evidenced in previous researches, during post-earthquake surveys or in experimental campaigns performed on existing constructions [6–9]. In this latter case, which is a typical situation when dealing with poor-quality mortars, even if the diagonal cracking is the leading failure mode, the activation of a shear-sliding mechanism could be identified and can influence, to some extent, the shear capacity of the masonry panel.

The shear-sliding failure mode can usually be described by a Coulomb friction model, considering the distinction between an initial Coulomb friction failure criterion and a residual one, the latter corresponding to a dry friction condition after cohesion softening [10]. In this framework, the local properties of the brick-mortar interface, in terms of initial shear strength, alternatively denoted as cohesion, and friction coefficient, are the key parameters to be evaluated. Experimental tests may be performed with this purpose both in laboratory and in-situ. Among different laboratory testing methods proposed and studied in the past [11–16], the standard triplet test [17] is often performed nowadays since it allows to best reproduce the desired shear-sliding failure and to obtain reliable results [18,19]. When dealing with existing constructions, slightly-destructive tests can be performed in-situ to evaluate the shear-sliding resistance of mortar joints [20,21]. Among these, the commonly used shove test, according to the ASTM Standard C1531 [22], consists in producing the sliding of a single brick, i.e. test unit, with respect to the surrounding masonry, along two horizontal mortar joints. The test provides an accurate estimation of the in-situ shear-sliding resistance, even though, strictly speaking, the sliding shear strength of the brick-mortar interface of a single unit is not the same as the shear strength of a masonry wall [21], even if a sliding mechanism is activated. However, information about the local properties of the brick-mortar interface should be reliably evaluated since they can be crucial in influencing the global failure mode and the shear

* Corresponding author.
E-mail addresses: francesca.ferretti10@unibo.it (F. Ferretti), S.Jafari@tudelft.nl (S. Jafari), R.Esposito@tudelft.nl (R. Esposito), J.G.Rots@tudelft.nl (J.G. Rots), claudio.mazzotti@unibo.it (C. Mazzotti).

https://doi.org/10.1016/j.engstruct.2022.113860
Received 1 August 2021; Received in revised form 21 December 2021; Accepted 6 January 2022
Available online 21 January 2022

strength of a masonry structural element.

The shove test, as reported in the ASTM Standard C1531 [22], can be performed according to three methods (Fig. 1), which differ in the way in which the vertical compression is controlled or applied. In *Method A*, the vertical compression is directly applied by means of two flatjacks, positioned above and below the test unit (Fig. 1a), while in *Method B* and *C*, the vertical stress is evaluated through an estimation of the acting dead and live loads (Fig. 1b and c, respectively).

In *Method A*, after the seating of the flatjacks, two bricks are removed from opposite ends of the chosen test unit and a hydraulic jack is inserted in one of the holes. At the beginning of the shove test, the pressure in the two flatjacks must be set to a very low value ($\leq$0.07 MPa). Then, the pressure in the horizontal jack is increased gradually until the sliding failure of the test unit is reached. During the tests, horizontal displacements should be measured using Linear Variable Differential Transducers (LVDT). After obtaining the first sliding, the pressure in the flatjacks is increased and the sliding is produced again. This process can be repeated several times and the shear strength (τ_i) at each vertical compressive stress level can be obtained by performing the ratio between the maximum shear load applied by the horizontal jack at the *i-th* vertical compressive stress level σ_i, and the total area of upper and lower bed joints.

According to the ASTM Standard [22], the coefficient of friction and the initial shear strength can be determined by performing a linear interpolation of the failure points (σ_i; τ_i) obtained at each vertical compressive stress level, plotted in a shear stress τ *vs* vertical compressive stress σ diagram. The testing procedure for *Method A* is the most complicated one from a practical point of view. However, the compressive stress level is controlled for the entire duration of the test and, if additional single and double flatjack tests are executed prior to the shove test, the state of stress and the deformability properties of masonry can be evaluated as well.

For *Method B* and *Method C*, the vertical load is estimated through load analysis and the chosen test unit is displaced horizontally using a hydraulic jack or a vertical jack. The horizontal force required to produce the first displacement of the brick provides a measure of the mortar joint shear strength. In these cases, only one failure point (σ; τ) is obtained, as σ now relates to the single case of existing vertical in-situ stress. Therefore, in order to calibrate a Coulomb friction failure domain, assumptions on the friction coefficient should be made or more than one test should be performed on the same masonry typology, e.g., for different in-situ stress levels.

Advantages of *Method A* with respect to *Method B* and *C* are related to the possibility of performing the test more than once at a single location, with different pre-compression. In this way, a reliable estimation of the failure criterion can be obtained. Moreover, the execution of the test according to *Method A* is equivalent to performing multiple shove tests with *Method B* or *C* at different building elevations (i.e. at different compressive vertical stress levels), if the masonry quality is quite uniform throughout the building [21]. However, the execution of the test is more complex and creates a greater disturbance of the stress pattern within the tested masonry portion, due to the creation of the flatjack slots.

Two main issues should be remarked regarding the execution of the shove test and the elaboration of the corresponding results. Firstly, for all the testing methods, there are uncertainties about the definition of the vertical compressive stress acting on the test unit, as highlighted also in previous researches [23–25]. Indeed, the actual stress distribution

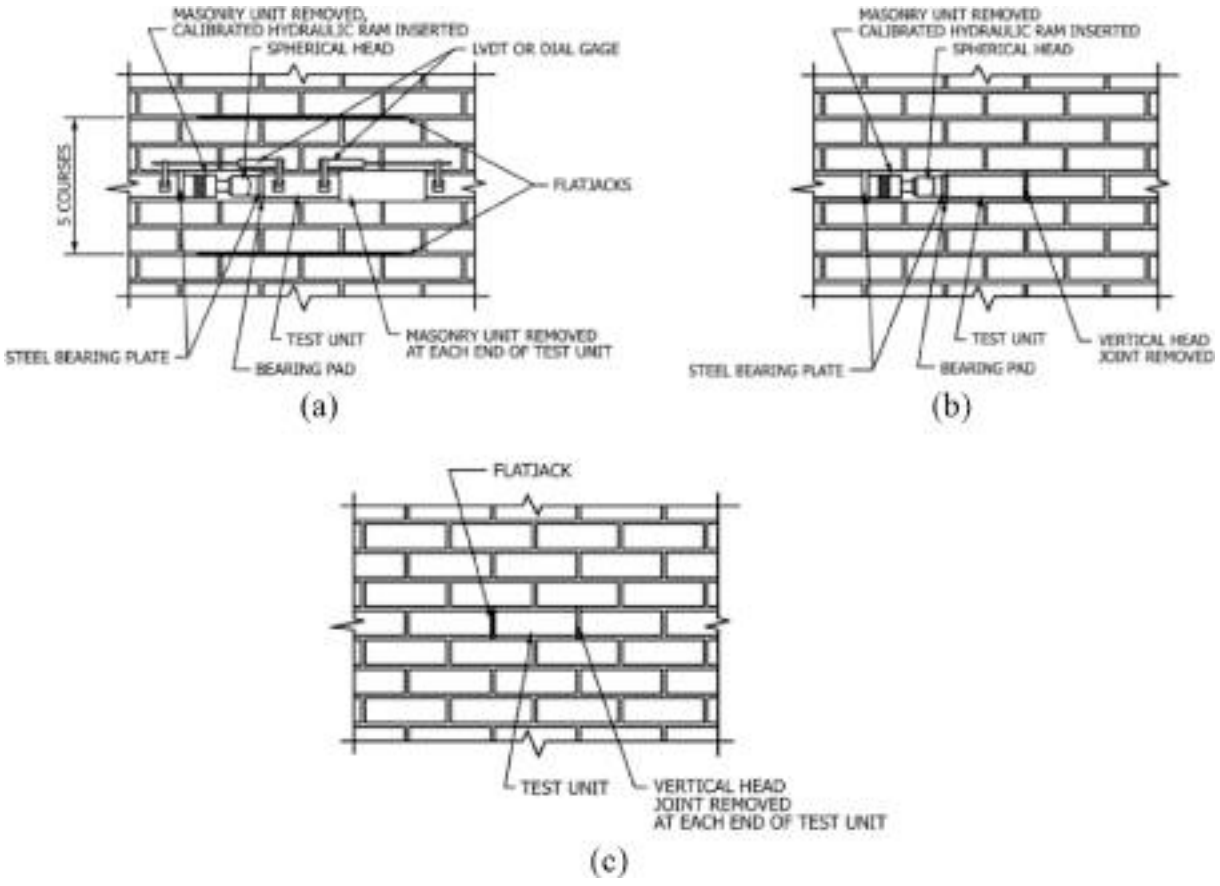

Fig. 1. Shove test setups [22]: (a) *Method A* with controlled vertical compression via flat jacks and horizontal shearing via hydraulic jack, with two bricks removed; (b) *Method B* with in-situ vertical compression and horizontal shearing via hydraulic jack, with one brick and one head joint removed; (c) *Method C* with in-situ vertical compression and horizontal shearing via flat jack, with only two head joints removed.

could significantly differ from the assumed uniform one imposed by the flatjacks (*Method A*) or estimated through load analysis (*Method B* and *C*). This can be due to several factors, such as the wall geometry (e.g. single-wythe or double-wythe), the removal of bricks adjacent to the test unit, the dilatant behavior of masonry, etc. For these reasons, only for *Method A* the ASTM Standard suggests the use of a modification factor, to be determined case by case, to convert the flatjack stress into vertical compressive stress on the test unit. Secondly, for *Method A*, it is not well specified in the Standard that the first failure condition is associated with an initial Coulomb friction failure criterion while the following ones – with increased vertical compressive stress – describe a pure frictional behavior of the bed joints and must be related to a residual Coulomb friction domain.

Many parameters play a role in the shear-sliding behavior observed in the mentioned experimental tests, such as the boundary conditions, the uniformity of the stress distributions along the mortar joints, the cracking formation and evolution, the dilatancy. In particular, the accurate study of the dilatant behavior of masonry is a very important aspect when performing shear tests. Dilatancy indicates an expansion (uplift) upon shearing, and it represents an important feature of masonry, highly relevant in case of confinement: if the expansion is prevented, a wedging effect is created, causing an increase in the vertical compressive stress. According to the Coulomb friction failure criterion, this phenomenon can lead to a significant shear strength increase [10,26,27]. Few researches only were conducted to evaluate the contribution of dilatancy to the shear strength of masonry samples, by combining experimental and numerical results of triplet tests and shove tests, and they led to the proposal of a different interpretation of the results of the shove test, conducted according to *Method A* [23–25]. It should be also mentioned that different outcomes could be observed from the triplet test and the shove test carried out on the same masonry typology [25,28]. Typically, higher results, in terms of shear strength, were found from the shove test with respect to the triplet test, for the same nominal value of vertical compressive stress applied to the sliding brick. This can be related to the differences between the actual and the nominal vertical compressive stress on the test unit during the shove test [20,24], which will be better analyzed in the following. Since the two tests were introduced to capture the same shear-sliding behavior, there is the need of assessing which factors, and to what extent, determine these discrepancies in the test outcomes.

The main objective of this paper is the study of the aspects and parameters that can affect the shear-sliding behavior of masonry during the shove test, by performing nonlinear numerical simulations with a brick-to-brick model, using the software DIANA FEA. The 2D numerical models are calibrated and validated thorough comparison with laboratory experimental results; a parametric analysis on dilatancy is also conducted. Considering the results of the numerical analyses, the issues previously mentioned will be discussed throughout the paper and further proposals to improve the shove test execution and result interpretation will be presented.

2. Numerical modeling

Masonry is a composite, non-homogeneous and anisotropic material, which exhibits a strong nonlinear behavior. Due to its intrinsic complexity, there is often the need of using robust numerical tools to study and analyze the behavior of masonry elements. Within the framework of detailed nonlinear analyses, a variety of possibilities exists concerning the description of masonry structures and different modeling strategies and constitutive models were proposed and developed in the past [1,29–33]. If a very accurate representation of masonry is needed – e.g. for small scale problems or for the study of local phenomena – the single components, i.e. bricks and mortar, can be modeled separately. In this case, a very detailed description of the materials is needed, whose properties are identified through laboratory tests on the masonry constituents or on small scale masonry samples.

With the aim of studying the shear-sliding behavior along a mortar joint in the shove test, a high level of accuracy is needed. Therefore, given also the relatively small dimensions of the specimens, a brick-to-brick modeling strategy was chosen. According to this strategy, denoted as simplified micro-modeling in previous researches [26,30], the mortar joints were modeled as zero-thickness interface elements and the brick units were modeled by using continuum elements with expanded geometry, so that the overall dimensions of the sample were unchanged [26]. To reduce the numerical burden without impairing the reliability of results, nonlinearities were only assigned to specific interface elements, while the bricks were considered to behave linear elastically. Both *Method A* and *Method B* of developing the shove test [22] were modelled to analyze and discuss their main differences. Details about the numerical model, its calibration and validation, are reported in the following sections.

2.1. Brick-to-brick model

The numerical analyses of the shove test presented in this paper were carried out by considering a full-scale, single-wythe, calcium silicate masonry panel, having dimensions of $2006 \times 3290 \times 102\ mm^3$. With the aim of calibrating and validating the numerical model, the materials, the wall geometry and the test setup were chosen to be equal to the ones adopted in a laboratory experimental campaign conducted at Delft University of Technology [34], in which the shove tests were performed according to the *Method A,* trying to reproduce as closely as possible the in-situ conditions of the test (Fig. 2).

The detail of the mesh used in the numerical model simulating the *Method A* of the shove test is shown in Fig. 3a,b. Mesh sensitivity analyses were performed to determine the dimensions of the finite elements, appropriate in terms of a balance between efficiency and accuracy: each brick was modelled by using 32 elements (mesh size $21 \times 28\ mm^2$). To better investigate the stress pattern outside the tested masonry portion, the entire wall was modeled maintaining the same mesh fineness. Given the geometry of the masonry panel, which was a single-wythe wall, a 2D model was considered adequate to reproduce the testing conditions. According to the adopted simplified micro-modeling approach, bricks were singularly modeled by using quadrilateral 8-noded plane stress elements, while 3+3-noded line interface elements were adopted to model the zero-thickness mortar joints, both vertical and horizontal. The wall was considered clamped at the base. At the top of the wall, the steel beam was not specifically modeled, but tyings (i.e. linear dependencies between nodal degrees of freedom) were adopted to force the nodes of the top cross section to displace equally in the vertical direction. Horizontal displacements on the top cross section were not restrained. The assumption about the horizontality of the top cross section of the wall was verified by performing preliminary numerical simulations, either modeling the rigid behavior of the beam with tyings or considering the proper flexural stiffness of the beam. Since similar results were obtained in the two cases, both in terms of stress distributions and shear strength, the assumption of rigid steel beam was considered adequate. To reproduce the presence of the steel bearing plates between the horizontal hydraulic jack and the bricks, tyings were adopted along the loaded lateral surfaces of the bricks as well to force the nodes to displace equally in the horizontal direction.

A linear elastic behavior was considered for the plane stress elements, modeling the bricks. The constitutive behavior of interface elements in the linear elastic range can be described as:

$$\begin{bmatrix} \sigma \\ \tau \end{bmatrix} = \begin{bmatrix} k_n & 0 \\ 0 & k_t \end{bmatrix} \cdot \begin{bmatrix} u \\ v \end{bmatrix} \tag{1}$$

where σ and τ are the normal and shear stresses along the interface, also known in literature as normal and shear tractions [26,29,30], k_n and k_t are the normal and the shear stiffness, respectively, and u and v are the normal and shear relative displacements. Within the adopted modeling

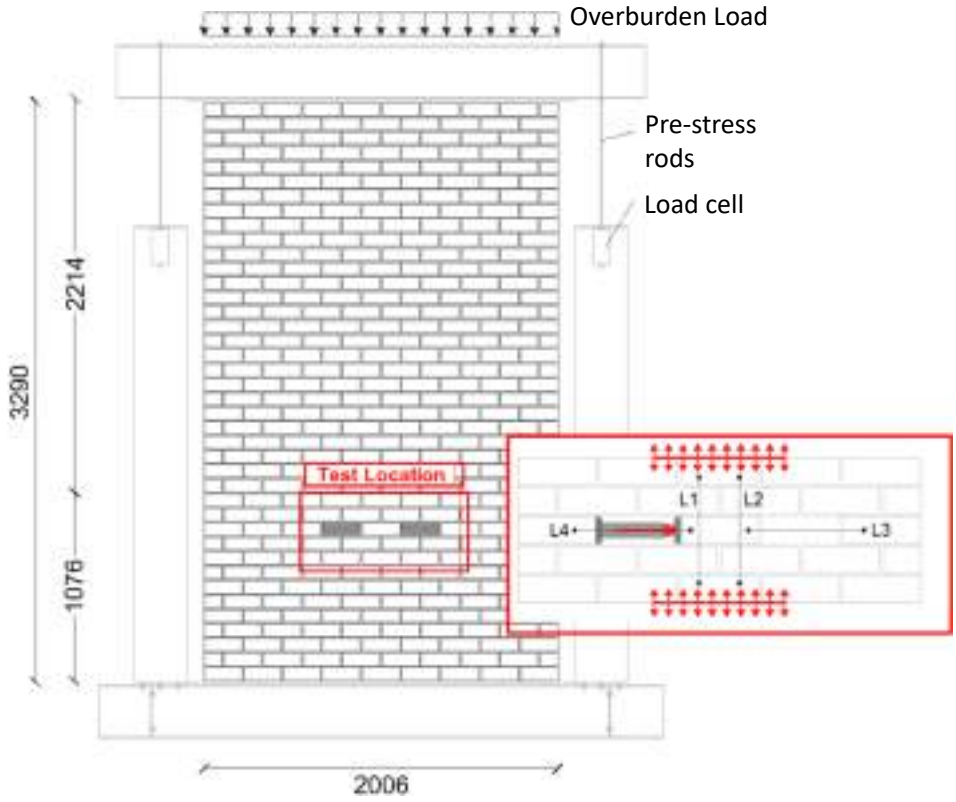

Fig. 2. Shove test – *Method A*: wall geometry and test setup.

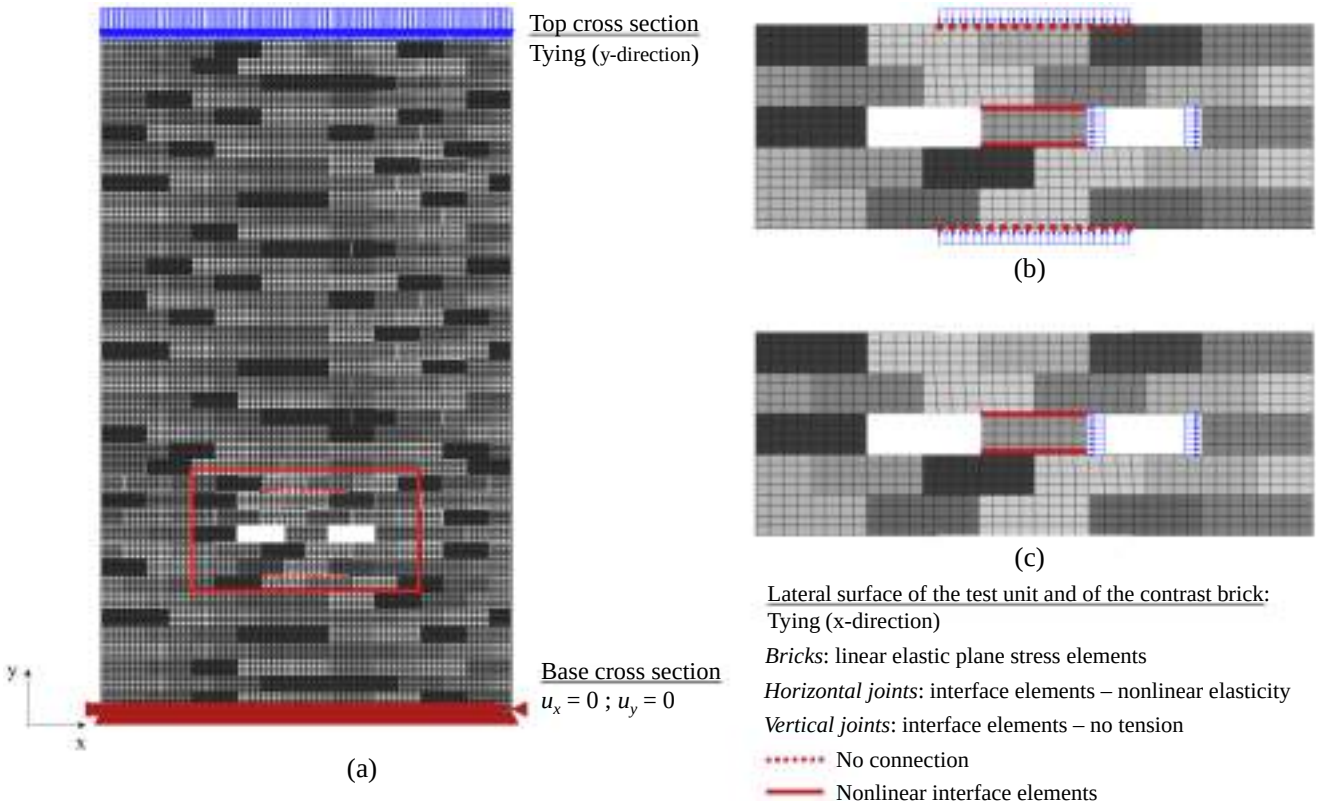

Fig. 3. Finite element model of the shove test: (a,b) *Method A*, with flatjacks, (c) *Method B*, without flatjacks.

strategy, the elastic stiffness parameters of the brick-mortar interfaces were evaluated by considering the mechanical properties and the actual dimensions of units and mortar joints as [26]:

$$k_n = \frac{E_b E_m}{t_m(E_b - E_m)}$$
$$k_t = \frac{G_b G_m}{t_m(G_b - G_m)} \quad (2)$$

where E_b and G_b are the elastic and shear modulus of the bricks, E_m and G_m are the elastic and shear modulus of the mortar, and t_m is the mortar joint thickness, in this case equal to 10 mm.

Since neither cracking nor failure was expected from brick units during the shove test, as confirmed by experimental observations (see Section 5), the nonlinear behavior was assigned only to the interface elements that modeled the mortar joints. More in detail, for all the horizontal mortar joints but those connected to the test unit and for all the vertical joints, direct uncoupled nonlinear-elastic relations were used. For the horizontal ones, a constant normal stiffness in compression and a tensile stiffness progressively reducing was adopted. In particular, the normal stiffness was set to zero when a tensile normal relative displacement equal to 0.001 mm was reached, which for a normal stiffness of 122.1 N/mm^3 corresponds to a tensile strength of 0.12 N/mm^2; this tensile strength value is equal to the value of the bond strength obtained by performing bond wrench tests on the investigated masonry typology [35]. Vertical joints, instead, were modeled as a fully no-tension material, i.e. the tensile strength was assumed to be zero. The choice of assigning weaker properties to the vertical joints was justified by considering that they are not subject to vertical loads during the curing, thus micro-cracks or even loss of bond between bricks and mortar are often present in these joints. No connections were considered between the edges of the flatjack holes, characterized by a length of 360 mm.

For the horizontal interface elements above and below the test unit, along which the sliding failure takes place, a composite interface model [30] was adopted. The composite interface model, also known as combined cracking-shearing-crushing model, was formulated in the context of multi-surface plasticity, including all failure mechanisms which can characterize the masonry behavior: tensile failure (Mode I), shear failure (Mode II), and compressive failure. A Coulomb friction failure criterion was assumed for shear, with a tension cut-off and an elliptical compressive cap. Both the tensile failure mode and the shear failure mode were characterized by an exponential post-peak softening behavior, as observed in experimental tests [10]. The compressive failure, instead, is characterized by a hardening–softening behavior. The reader can refer to previous researches [27,30,36] for the complete description of the numerical implementation.

In the following, the model adopted to describe the mode-II shear failure is described in detail, starting from the well-known linear function of the Coulomb friction yield criterion:

$$f(\sigma, \kappa_2) = |\tau| + \sigma tan\phi(\kappa_2) - c(\kappa_2) \quad (3)$$

in which the cohesion and friction softening are defined through the following expressions:

$$c(\kappa_2) = c_0 \cdot exp\left(-\frac{c_0}{G_f^{II}}\kappa_2\right) \quad (4)$$

$$tan\phi(\kappa_2) = tan\phi_0 + (tan\phi_{res} - tan\phi_0)\frac{c_0 - c(\kappa_2)}{c_0} \quad (5)$$

In the previous equations, c_0 is the cohesion of the brick-mortar interface, ϕ_0 and ϕ_{res} are the initial and the residual friction angle, respectively, G_f^{II} is the mode-II fracture energy, and κ_2 is the shear plastic displacement. Exponential softening is assumed for both the cohesion c and the friction angle φ. In particular, the friction softening is taken proportional to the cohesion softening. Under these hypotheses, the mode-II fracture energy increases as the normal compressive stress level increases, as confirmed experimentally [26,37].

Non-associated plasticity [38] is here considered, given that masonry joints are characterized by a friction angle that is usually significantly higher than the dilatancy angle, defined as the angle between the normal and shear relative plastic displacements along the sliding interface. Therefore, a non-associated plastic potential g_2 is defined, with a dilatancy angle ψ and a strain softening hypothesis:

$$g_2 = |\tau| + \sigma tan\psi - c_0 \quad (6)$$

In the computational implementation of the model, according to the proposal by Van Zijl [27], who improved previous formulations [30,39], a variable dilatancy is considered. This was done to accurately capture the pressure buildup and the corresponding shear strength increase. Indeed, it was demonstrated in several experimental works that dilatancy tends to zero upon increasing shear displacement and increasing normal confining stress. Accordingly, the plastic normal displacement u_{pl} component depends on the confining stress σ and on the plastic shear slip v_{pl}, through the expression:

$$u_{pl} = \frac{\Psi_0}{\delta}\left\langle 1 - \frac{\sigma}{\sigma_u}\right\rangle (1 - e^{-\delta \cdot v_{pl}}) \quad (7)$$

where $\Psi_0 = \tan\psi_0$ is the dilatancy at zero confining stress and shear-slip, σ_u is the confining compressive stress at which the dilatancy becomes zero, and δ is the dilatancy shear slip degradation coefficient. Consequently, the dilatancy can be expressed as a function of the same parameters:

$$\Psi = \Psi_0\left\langle 1 - \frac{\sigma}{\sigma_u}\right\rangle e^{-\delta \cdot v_{pl}} \quad (8)$$

From previous expressions, which reflect experimental observations [10], it can be noticed that, given a constant confining stress σ, the rate of plastic normal displacement decreases exponentially with plastic shear slip.

The input parameters used for masonry in the numerical models were calibrated on the basis of experimental tests on small scale samples, as described in Section 2.2. The numerical simulations were performed by means of the finite element software DIANA FEA (Release 10.1). Phased analyses were carried out to exactly reproduce the testing procedure:

- Phase 1: application of the self-weight and the overburden;
- Phase 2: execution of the first slot for the seating of the superior flatjack;
- Phase 3: execution of the second slot for the seating of the inferior flatjack;
- Phase 4: removal of the bricks adjacent to the test unit;
- Phase 5: application of the flatjack pressure;
- Phase 6: application of the shear load.

The nonlinear analyses were performed considering quasi-static loading conditions, by imposing an increasing horizontal force both to the sliding brick (test unit) and to the contrast brick, to reproduce the presence of the horizontal hydraulic jack (Fig. 3). A regular Newton-Raphson method and arc-length with updated normal plane method were adopted to control the nonlinear problem solution.

Modeling choices similar to the ones just described were adopted also for the numerical simulations of the shove test according to *Method B*, with the only difference being the absence of the flatjack holes, that is considering the continuity of masonry above and below the test unit (Fig. 3c).

2.2. Calibration of the model against triplet tests

For the calibration of the mechanical parameters of the masonry

components and of the combined cracking-shearing-crushing model adopted to simulate the nonlinear behavior of the interface elements, the results of an experimental campaign performed on calcium silicate brick masonry were considered. Standard laboratory tests were conducted for the mechanical characterization of bricks and mortar [40], and 10 standard triplet tests were performed [17] on specimens built by using calcium silicate bricks (214 × 102 × 72 mm^3) and pre-mixed cementitious mortar (class M5), with joint thickness of 10 mm.

The triplet test setup is reported in Fig. 4. The lateral pre-compression load F_p (producing a normal stress along the mortar joints) was applied by means of a manually operated hydraulic jack and kept constant throughout the test. The shear load F was then applied to the central brick by using a displacement-controlled apparatus with a hydraulic jack, having capacity of 100 kN. The shear displacement rate was equal to 0.005 mm/s during the loading phase and to 0.05 mm/s in the unloading phase. Different pre-compression values were adopted: 0.05, 0.20, 0.60, 1.20 MPa. For all the pre-compression levels, after the attainment of the first brick sliding, the pre-compression load was increased up to maximum three times with increments of 0.10 ± 0.05 MPa and the frictional relative shear-slip between the unbonded surfaces was continued. This procedure, similar to the one adopted in the shove test, was repeated several times to obtain a better estimation of the residual Coulomb friction criterion. During the test, displacements tangential (shear) and orthogonal (normal) to the mortar joints were measured by means of six LVDTs, positioned on both sides of the specimen and indicated as L_1, L_2 and L_3 (for one side only) in Fig. 4.

The experimental results of the triplet tests are reported in Fig. 5, in terms of shear stress τ *vs* shear displacement δv and in terms of normal displacement δu *vs* shear displacement δv. The typical shear behavior (Fig. 5a) was characterized by an initial linear branch up to the peak load, followed by a softening phase and a residual plateau, corresponding to a dry friction condition. Further pre-compression stress increments produced corresponding plateau at higher levels of shear stress. Concerning the dilatant behavior of the specimens (Fig. 5b), it can be clearly noticed that the normal displacement δu, indicating lateral expansion if positive, decreased as the pre-compression stress increased and, as expected, it became stable in correspondence with large shear displacements [27]. When negative normal displacements were registered, i.e. for high pre-compression values, they were associated to local mortar crushing and compression nonlinearity within the joint thickness.

The mechanical parameters needed to describe the combined cracking-shearing-crushing model, reported in Table 1, were either obtained from experimental results or calibrated according to available formulations. More in detail, the elastic properties of bricks and mortar, from which the interface stiffness coefficients k_n and k_t were calculated

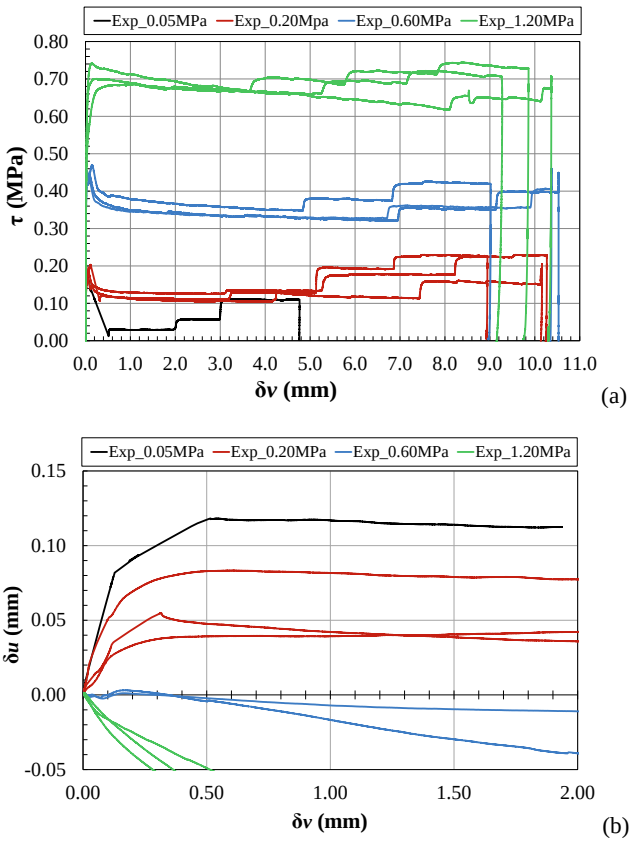

Fig. 5. Standard triplet test results: (a) shear stress *vs* shear displacement of the central brick; (b) normal displacement *vs* shear displacement.

according to Equation (2), were determined from the results of standard laboratory tests on the constituents and on masonry wallets: first, the elastic modulus of bricks was obtained from uniaxial compression tests [41], by measuring vertical deformations; then, the results of uniaxial compression tests on wallets [42] were considered to indirectly determine both the elastic modulus of the mortar and the Poisson's ratios of bricks and mortar. The triplet test results were used to evaluate the parameters related to the shearing mode (Mode II). By performing linear interpolations of the (σ_i, τ_i) points for all the pre-compression levels, the Coulomb friction failure criterion was obtained, both at the peak (c_0, ϕ_0) and in the residual phase (c_{res}, ϕ_{res}). The mode-II fracture energy G_f^{II} was evaluated for each test and its linear dependence on the pre-compression

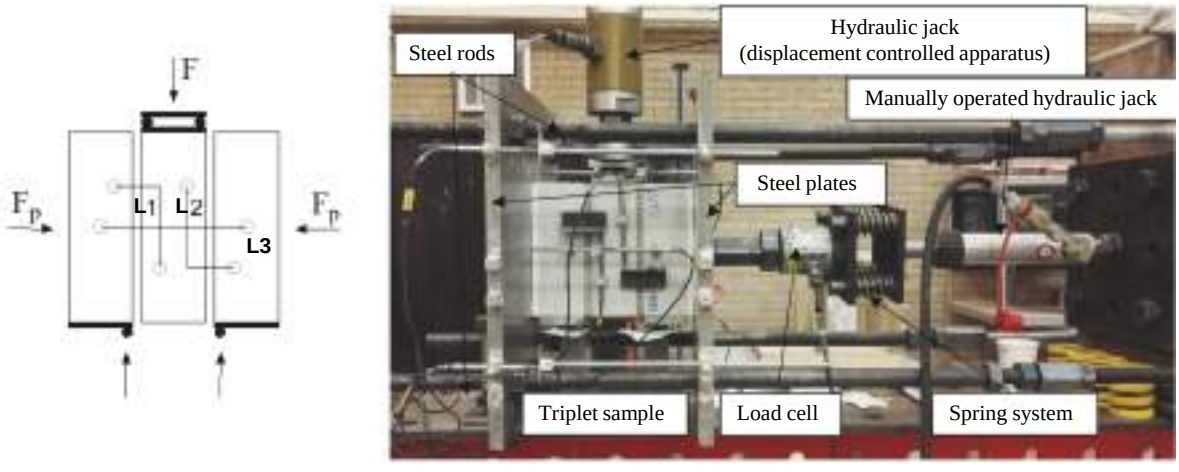

Fig. 4. Standard triplet test: experimental setup.

Table 1
Input parameters for the elastic bricks and the nonlinear joint interface elements.

Mechanical parameter	Symbol	Units	Value	Obtained from tests	Calibrated
Elastic modulus of brick	E_b	N/mm^2	10000	✓	
Poisson's ratio of brick	ν_b	–	0.16		✓
Elastic modulus of mortar	E_m	N/mm^2	1088		✓
Poisson's ratio of mortar	ν_m	–	0.20		✓
Interface normal stiffness	k_n	N/mm^3	122.1		✓
Interface shear stiffness	k_t	N/mm^3	50.7		✓
Tensile strength	f_t	N/mm^2	0.09		✓
Mode-I fracture energy	G_f^I	N/mm	0.01		✓
Cohesion	c_0	N/mm^2	0.13	✓	
Friction angle	ϕ_0	°	26.5	✓	
Residual friction angle	ϕ_{res}	°	26.5	✓	
Dilatancy angle	ψ_0	°	21.4		✓
Confining normal stress	σ_u	N/mm^2	0.58		✓
Exp. degradation coeff.	δ	–	9.63		✓
Mode-II fracture energy $\left(G_f^{II} = a\sigma + b\right)$	a	mm	0.114		✓
	b	N/mm	0.011		✓
Compressive strength	f_c	N/mm^2	6.35	✓	
Compr. fracture energy	G_f^c	N/mm	20	✓	
Equiv. plastic shear displ.	κ_p	–	0.005	✓	

stress level, according to previous studies [10,26], was confirmed: the coefficients a and b reported in Table 1 were calibrated from a linear regression of the experimental data. Parameters governing the dilatant behavior of mortar joints were evaluated by least-squares fitting of the experimental data of Fig. 5b, according to the formulation for dilatancy introduced in Section 2.1 and accounting for the presence of two mortar joints involved in the shear-sliding failure [27]. With reference to the tensile failure (Mode I), tensile strength was determined as 2/3 of the cohesion and mode-I fracture energy was considered equal to the 10% of the mode-II fracture energy, according to indications found in previous studies [26]. The parameters describing the crushing failure mode, i.e. the compressive cap, were obtained by considering the results of standard compression tests on masonry wallets.

It is worth mentioning that, in the cited experimental program, besides standard triplet specimens, arranged in a stacked bond, also modified triplet specimens, characterized by a running bond pattern, were tested with the aim of evaluating the influence of the presence of the vertical mortar joints on the shear-sliding behavior of the investigated masonry. This situation is actually more similar to the one usually encountered when performing the shove test in-situ. No significant difference was observed in terms of shear parameters obtained from test on modified and standard triplets, as reported in [37].

Numerical simulations were carried out to analyze the capability of the calibrated model to describe the shear-sliding behavior of triplet specimens. The model was validated through comparisons between numerical and experimental results for modified triplet specimens, which are presented in Fig. 6, both in terms of shear stress τ *vs* shear displacement δv and in terms of normal displacement δu *vs* shear displacement δv. The scatter registered for the normal displacements

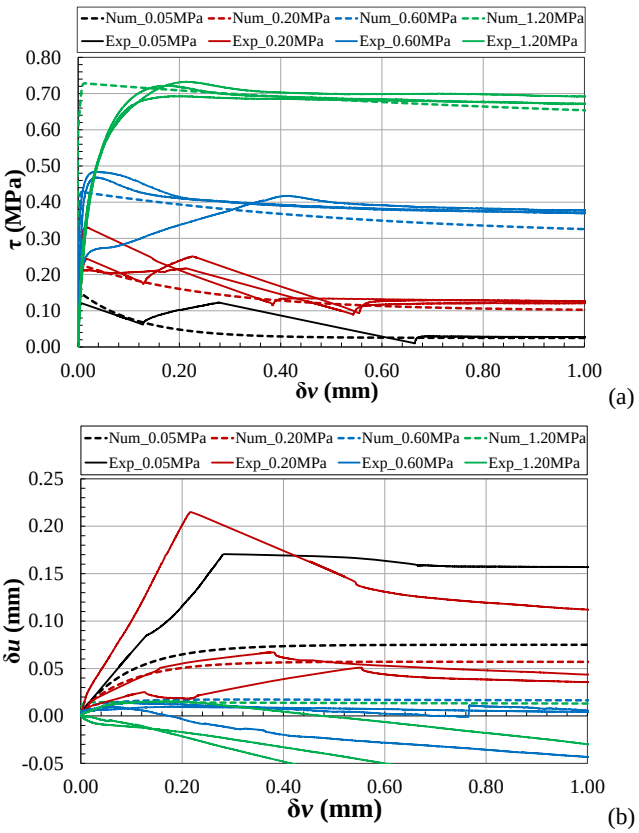

Fig. 6. Comparison between numerical and experimental results for modified triplet test: (a) shear stress *vs* shear displacement of the central brick; (b) normal displacement *vs* shear displacement.

measured experimentally (Fig. 6b) can be associated to the specific development of the sliding failure and to the fact that a single measurement in the middle of the specimen is here adopted to describe its entire lateral response. In addition, being these values quite small with respect to shear displacements, they can be very sensitive even to small experimental anomalies (e.g. small rotation of the plates). A very good agreement between experimental and numerical outcomes was obtained.

In general, for both standard and modified triplets, the numerical results allowed to gain a better insight about the behavior of the specimens (Fig. 7) and also to investigate the parameters which could mostly affect the results, i.e. boundary conditions and dilatancy. The predominant experimental failure mode, representatively shown in Fig. 7a, was characterized for all pre-compression levels by a shear failure at the brick-mortar interface without any damage to the bricks, and it was well captured by the numerical model. Local mortar crushing was observed in few tests only, typically for high pre-compression values, as shown in Fig. 7b. These findings represent a first signal of the potential of this model to accurately reproduce the shear-sliding failure of masonry. Stresses in the bricks were also checked to confirm the assumption about their elastic behavior. Further details about the triplet test results here presented, both from the experimental and the numerical point of view, can be found in [43].

3. Numerical results for shove test

The results of several numerical simulations, performed with reference to the numerical model related to both *Method A* and *Method B* of the shove test, are presented in this section. The material parameters according to Table 1, as calibrated against triplet tests on the same brick and mortar material, were used. The finite element representation was

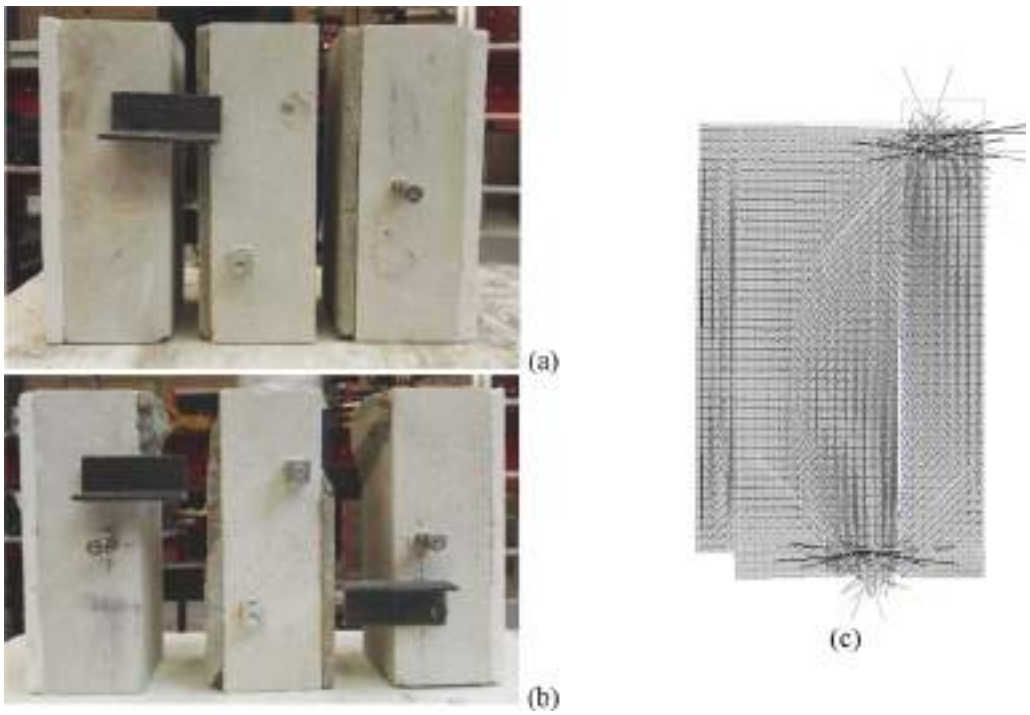

Fig. 7. Standard triplet test: (a) typical sliding failure mode; (b) shear failure with local mortar crushing; (c) deformed shape and principal stress distribution of the numerical model at pre-compression of 0.20 MPa - post-peak phase ($\delta_v = 0.08$ mm).

Table 2
Loading conditions for the numerical simulations.

Model	Shove test method	Vertical compressive stress* (MPa)	Flatjack pressure (MPa)
A1 – Low confinement	*Method A*	0.15	0.05
A2 – Medium confinement	*Method A*	0.25	0.05
A3 – High confinement	*Method A*	0.60	0.05
B1 – Low confinement	*Method B*	0.15	–
B2 – Medium confinement	*Method B*	0.25	–
B3 – High confinement	*Method B*	0.60	–

* Given by self-weight and overburden at the sliding brick height at the beginning of the test.

described in Section 2.1. Different loading conditions were considered (Table 2). In particular, for *Method* A, the same flatjack pressure – set to a very low value, as suggested by the ASTM Standard – was applied in all the simulations, while three different overburden loads were imposed at the top of the masonry wall to reproduce the presence of more than one floor above the tested area and, therefore, to analyze the influence of the acting vertical load on the test outcomes. For *Method B*, three loading conditions were chosen by simply varying the overburden loads, as done for *Method A,* with the objective of studying the differences between the two methodologies, supposing that the shove tests are performed in the same location of an existing masonry wall, i.e. with the same acting overburden load.

3.1. Shove test results – Method A

The results of the three numerical simulations performed by considering the *Method A* of the shove test are presented in Fig. 8a,b,

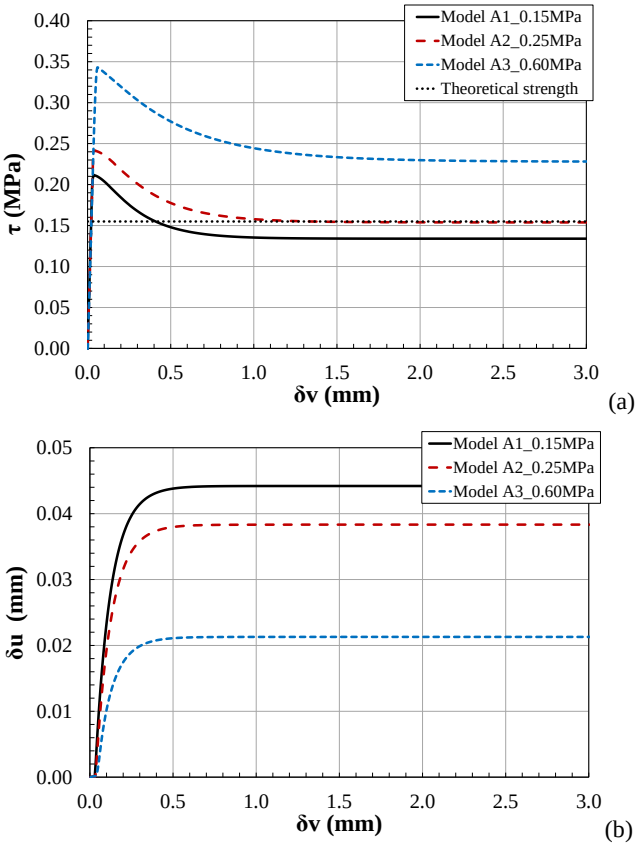

Fig. 8. Shove test results – *Method A*: (a) shear stress τ *vs* shear displacement δv; (b) normal displacement δu *vs* shear displacement δv.

respectively in terms of shear stress τ *vs* shear displacement δv and normal displacement δu *vs* shear displacement δv. To build the reported graphs, the shear stress was evaluated at each instant of the analyses, i.e. for each load increment F_i. The shear displacement δv represents the relative displacement of the test unit with respect to the surrounding masonry, while the normal displacement δu is evaluated as the average of the difference between the vertical displacement of two pairs of points, positioned above and below the test unit, to investigate dilatancy. The nodes considered for the evaluation of these relative displacements were taken in correspondence of the LVDT gauge points, represented in Fig. 2.

From Fig. 8a, it can be noticed that the shear behavior was characterized, as already observed for the triplet tests, by an initial linear trend up to the peak load, followed by a softening branch and a residual dry-friction phase, growing with the overburden. In Fig. 8b, the presence of a positive displacement δu indicates a vertical expansion upon shearing, which could reveal that the uplift is not restrained. The graph in Fig. 8b was not built by considering the plastic components of the displacements, as could be expected looking at the dilatancy formulation, but by considering the total normal and shear displacements: this representation is more practical and can be directly compared with results from experimental tests.

It is worth mentioning that, for all the models, the condition in which the failure domain is reached for all the integration points of the sliding

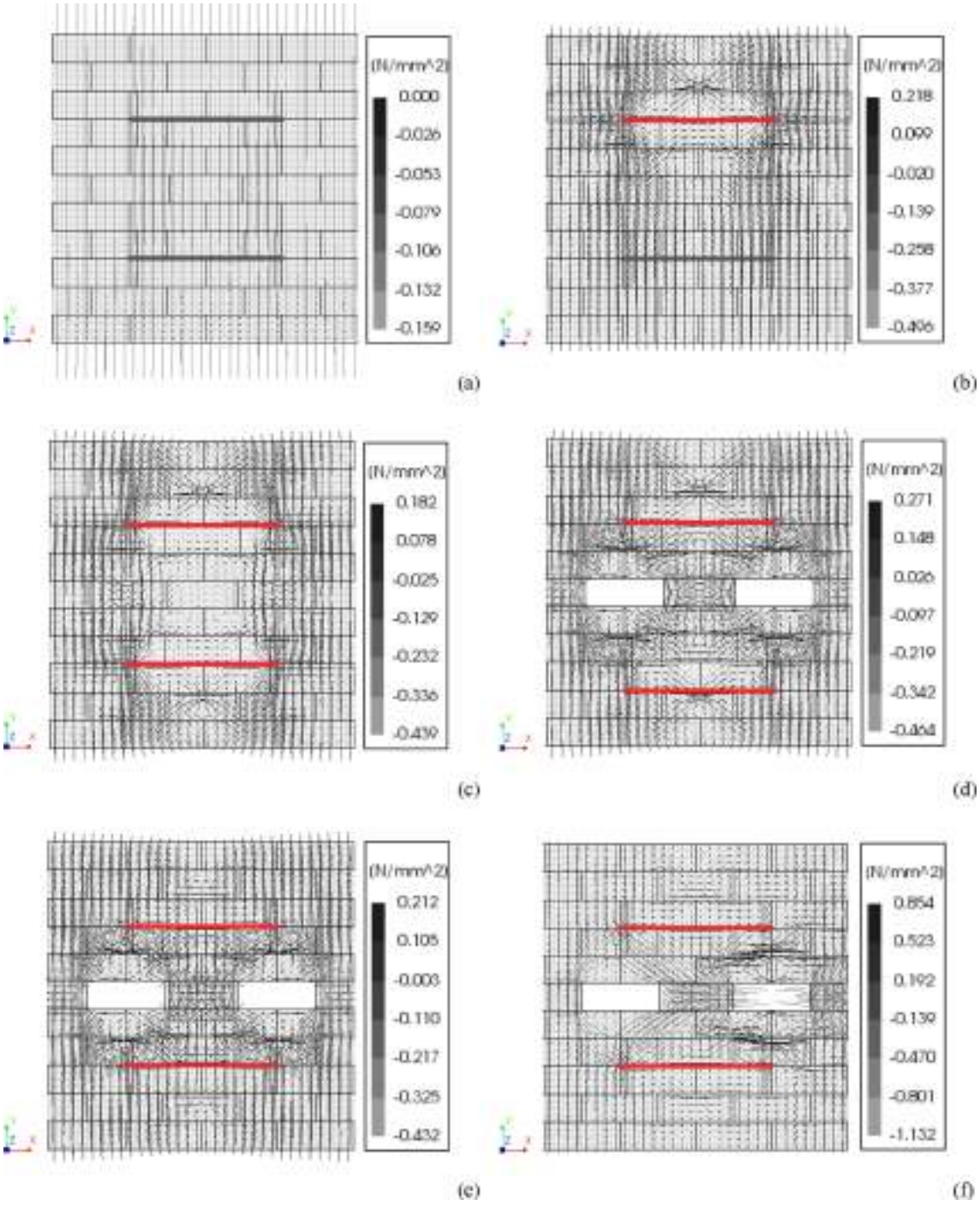

Fig. 9. Model A1 – In-plane principal stresses distributions: (a) self-weight and overburden application; (b) execution of the first slot; (c) execution of the second slot; (d) removal of the bricks; (e) application of the flatjack pressure; (f) shear load (peak).

surface, called "*shear crack initiation load*" in the following, corresponds to the peak load of the reported curves. This aspect, which could indicate a limited influence of dilatancy on the test results in terms of shear strength, will be further investigated in Section 4.

The numerical analyses revealed significant differences in the shear capacity, even if the same flatjack pressure was applied. In Fig. 8a, the theoretical shear strength, calculated according to the Coulomb friction model considering a vertical compressive stress value equal to the one applied by flatjacks (0.05 MPa), is reported for comparison; in all cases the obtained shear strength was significantly higher than the theoretical one. In particular, the higher the overburden load the higher the shear capacity and, correspondingly, the lower the vertical expansion δu. It became apparent that the average compressive stress on the sliding mortar joints was far away from being equal to the flatjack pressure and it was influenced by the presence of the overburden load and by the preceding phases of the test, e.g. execution of the flatjack slots and removal of the bricks. By looking at the evolution of the principal stresses within the tested masonry portion, represented in Fig. 9 for the Model A1, it is possible to observe the following:

- Phase 1 (Fig. 9a): the compression lines are vertical and the in-plane principal compressive stresses due to the self-weight and to the application of the overburden load are uniform on the cross section of the panel; the compressive stress in correspondence with the sliding brick is 0.15 MPa.
- Phase 2 (Fig. 9b): due to the execution of the first slot for the seating of the upper flatjack, the compression lines deviate from the vertical direction, creating a parabolic unloaded area above and below the slots.
- Phase 3 (Fig. 9c): due to the execution of the second slot for the seating of the lower flatjack, the compression lines deviate again from the vertical direction around the second slot and the whole masonry portion between the two flatjack slots results almost stress free.
- Phase 4 (Fig. 9d): the removal of the two bricks produces a strong variation in the principal stresses distribution: the compression stresses turn around the new holes, spreading over the lateral portions of the panel, and deviate also inside the stress-free area (see Phase 3), concentrating on the test unit and producing a strong stress intensity increase and stress concentrations at both joint edges.
- Phase 5 (Fig. 9e): after the application of the flatjack pressure, the compression lines between the two flatjacks are not vertical: they deviate partially on the test unit and partially outside the tested region, i.e. beyond the holes of the removed bricks. This effect is more evident for low flatjack pressure values and contributes to producing stress concentrations at the joint edges of the test unit.
- Phase 6 (Fig. 9f): the application of the horizontal shear load influences the in-plane principal stresses distribution, which results no more symmetric. Indeed, it causes a horizontal compression on the sliding brick, which is transferred, through the sliding interfaces, to the masonry portions above and below the test unit along inclined patterns. The diffusion of the shear load inside the masonry also produces a variation in the stress pattern along the sliding joints.

To better analyze the stress distributions along the sliding mortar joints, the normal and shear stress developments along the top sliding interface are reported in Fig. 10 for the Model A1. The steps already considered for the in-plane principal stresses distributions are here considered for the normal stress patterns (Fig. 10a). For the shear stresses (Fig. 10b), only the stress distributions at the peak load and in the residual phase are shown since they are null or negligible during the application of the vertical loads. With reference to the normal stress development, uniform distributions were associated with the application of the self-weight and the overburden load, as expected. Then, relaxation of the masonry portion between the two slots was registered, with decreasing compressive stresses along the interface, even tending

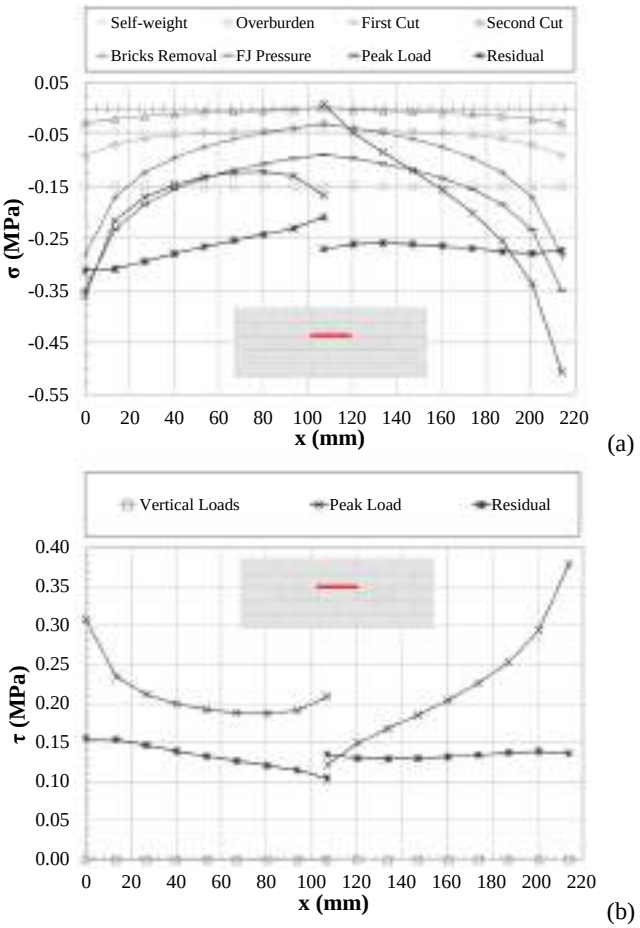

Fig. 10. Stress evolution along the top sliding interface for Model A1: (a) normal stress; (b) shear stress.

to zero after the execution of the second slot. Compressive stresses were slightly higher in this phase at the extremities of the sliding interface. Due to the removal of the bricks, the non-uniformity of the normal stress distributions became evident, with quite high compressive stresses at the extremities of the joint. An analogous situation was noticed with the application of the flatjacks pressure, which determined an increase of the compressive stress. When the shear load was applied – the step corresponding to the peak load is considered – the compressive stresses increased significantly on the right-end side of the sliding interface, close to the application of the shear load. On the left-end side, instead, the state of stress remained almost unchanged with respect to the previous phase. In the central portion of the joint, the discontinuity of the stress distributions is justified by the presence of the head joints above the interface. This determined, on one side of the head joint, a consistent decrease of the compressive stress, which became almost null or even positive; on the other side of the head joint, instead, a compression increase was noticed. From a qualitative point of view, in correspondence of the peak load, the shear stress distribution (Fig. 10b) was similar to the normal stress one, with higher shear stresses on the right-end side and a discontinuity in correspondence of the head joint. Smoother distributions can be observed in the residual phase, both for normal and shear stresses.

The results presented in Fig. 10 were also representative of the stress distributions for the bottom interface and showed, in a quite evident manner, the extreme complexity connected to the execution of the shove test according to the *Method A* proposed by the ASTM Standard. The observed trend is indeed similar for all the models A1, A2 and A3. Great uncertainties are related to the estimation of the compressive stress acting on the joints during the entire duration of the test. Due to the

cutting of the slots for the seating of the flatjacks and the removal of the bricks, the state of compression along the sliding interface is also affected by the presence of the compressive stress given by the overburden, which partially goes on the test unit. These observations support the results of the numerical simulations (Fig. 8), in which the increase of the overburden load is associated to an increase in the shear capacity.

3.2. Shove test results – method B

The results of the three numerical simulations performed by considering the *Method B* of the shove test are presented in Fig. 11 in terms of shear stress τ *vs* shear displacement δv and normal displacement δu *vs* shear displacement δv. The graphs of Fig. 11a are all characterized by an initial almost linear branch up to the shear crack initiation load, that corresponds to the point in which the failure domain is reached for all the integration points of the interface elements modeling the sliding mortar joints. Beyond the shear crack initiation load, a hardening branch is recognizable for Model B1, characterized by a peak load greater than the shear crack initiation load. For Model B2 and Model B3, instead, the shear crack initiation load and the peak load coincide. In all cases, after reaching of the peak load, a softening and a residual phase can be recognized. With reference to Fig. 11b, it is possible to observe that in the first part of the test, the masonry portion was subject to shortening. Then, as soon as the shear crack initiation load is reached, the normal displacement δu inverts its trend and a positive increase is registered for Model B1 and Model B2, indicating a volume expansion during the sliding of the test unit. For Model B3, in which the overburden load is higher than the confining compressive stress σ_u, the tested masonry portion remains contracted for the entire duration of the test. It should be mentioned that the obtained shear strength values were

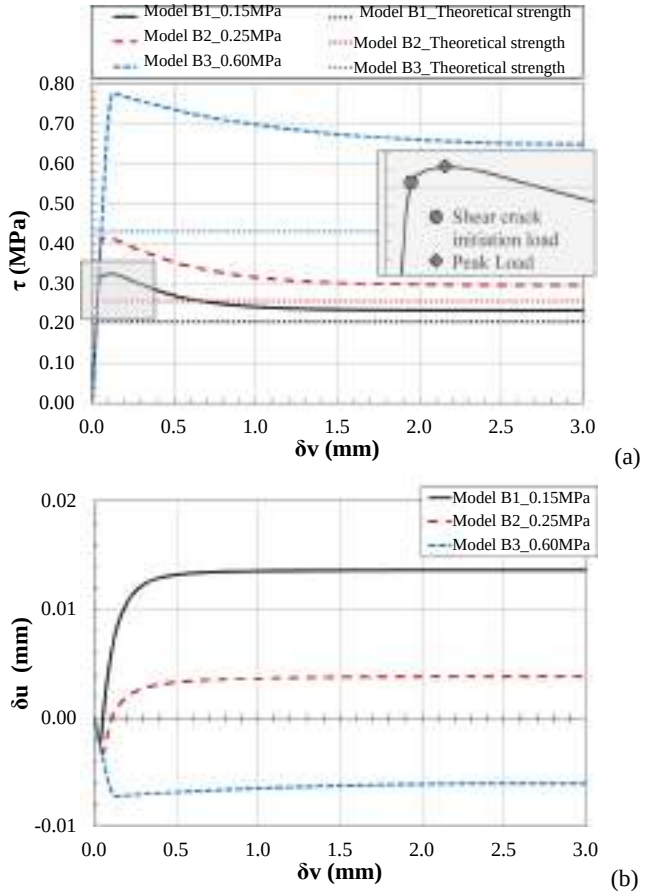

Fig. 11. Shove test results – *Method B*: (a) shear stress τ *vs* shear displacement δv; (b) normal displacement δu *vs* shear displacement δv.

always higher with respect to the theoretical ones (horizontal lines in Fig. 11a), calculated according to the Coulomb friction domain by considering vertical compressive stress values equal to the ones given by self-weight and overburden for the different models, indicating that the actual compressive stress value on the sliding joints was higher than the one given by the acting vertical load. It can be observed, in general, that the increase in the overburden load, directly influencing the compressive stress on the test unit, determines, on the one hand, an increase in the shear capacity and, on the other hand, an overall reduction in the normal expansion δu. This reduction mainly depends on the variable dilatancy formulation, i.e. dilatancy decreases as the compressive stress increases. Indeed, the elastic contraction of the brick due to the increased vertical compression has a negligible influence, especially in the post-peak phase.

With reference to the evolution of the in-plane principal stress distributions within the masonry portion subject to the shove test, presented in Fig. 12 for Model B1, it is possible to notice that, after the removal of the bricks, the vertical compression lines due to self-weight and overburden (Fig. 12a) deviated around the holes, producing a strong variation in the principal stress pattern and stress concentrations at the joint edges (Fig. 12b). Afterwards, the application of the shear load produced lateral compression on the sliding brick, which was transferred to the masonry above and below, determining a variation in the compressive stress along the sliding interfaces (Fig. 12c).

The normal and shear stress developments along the top sliding interface are reported in Fig. 13 for the Model B1. For the shear stresses, only the stress distributions at the shear crack initiation load, at the peak load, and in the residual phase are shown, since they are null or negligible during the application of the vertical loads. It was noticed that the normal stress distribution became non-uniform when the bricks were removed. In this phase, quite high compressive stresses were present along the interface, with stress concentrations at the extremities. With the application of the shear load corresponding to the failure of the interface (shear crack initiation load), the compressive stresses significantly increased on the right-end side, close to the application of the shear load. On the left-end side, instead, the state of stress remained almost unchanged with respect to the previous phase. As evidenced for *Method A*, the discontinuity of the stress distributions can be observed in correspondence with the head joint. Considering the step corresponding to the peak load, the compressive stress was still high on the right-end side of the joint, but a more uniform distribution can be recognized elsewhere. From a qualitative point of view, in correspondence of both the shear crack initiation load and the peak load, the shear stress distributions were similar to the normal stress ones. Smoother distributions can be observed in the residual phase, both for normal and shear stresses.

The results presented for the Model B1 shows the lower complexity of the shove test performed according to *Method B* with respect to *Method A*. However, also in this case, there are uncertainties related to the estimation of the compressive stress acting on the test unit during the entire duration of the test. The most important contribution to the compressive stress state was given by the vertical loads during the phase in which the bricks were removed.

4. Role of dilatancy and vertical loads

4.1. Parametric studies on dilatancy

With the objective of studying how dilatancy can affect the results of the shove test, according to both *Method A* and *B*, a series of parametric analyses were performed. In particular, according to the variable formulation for dilatancy proposed by Van Zijl [27] and used in this research, the dilatant behavior of masonry is governed by three parameters: the dilatancy angle at zero normal confining stress and shear slip (ψ_0), the confining compressive stress at which the dilatancy becomes zero (σ_u), and the dilatancy shear-slip degradation coefficient (δ).

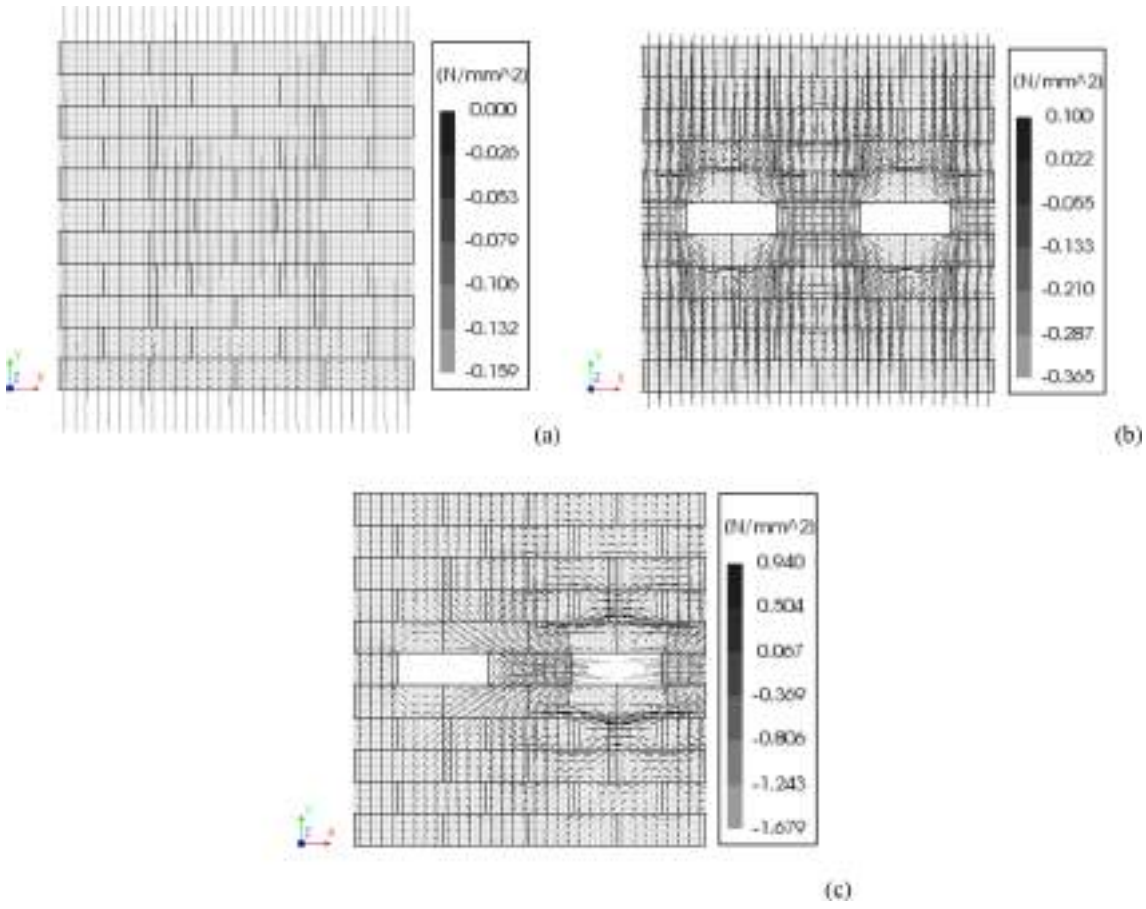

Fig. 12. Model B1 – In-plane principal stress distributions: (a) self-weight and overburden application; (b) removal of the bricks; (c) shear load (peak).

To analyze the effect that each parameter can have on the shear-sliding response of a masonry unit in the shove test, parametric studies were performed by varying one parameter at a time, leaving the others unchanged. In total, 8 parametric analyses were carried out for both testing methods, as reported in Table 3. More in detail, with respect to the reference values calibrated through the triplet test results, the parameters were changed in order to increase the role of dilatancy: greater values were chosen for ψ_0 and σ_u, while lower values were selected for δ. To be specific about the parametric analyses on ψ_0, the first chosen value was equal to the friction angle, while the second one was 1.5 times higher than the reference value. In this latter case, even if the initial dilatancy angle ψ_0 was higher than the friction angle, the thermodynamic consistency, as defined in [27], was respected throughout the analyses, given the variable dilatancy formulation (Equation (8)) and being the confining stress σ a negative (i.e. compression) and non-zero value on the sliding interfaces. In the following, the results will be presented for Model A1 and B1 only, given that for low compressive stress values the effect of dilatancy is more evident.

Before analyzing the results of the parametric analyses, it should be noticed that, in the numerical model of the shove test, the vertical displacements cannot be considered completely free. Indeed, even if the vertical translation is not constrained at the top of the panel, the masonry outside the tested region could act as a sort of impediment to the uplift along the sliding joints. Consequently, if volume expansion is restrained to some extent, increases in the compressive stress state on the sliding interfaces can be observed, leading to an increase in the shear strength.

The results of the parametric analyses are presented for *Method A* and *B* in Figs. 14 and 15, respectively, in terms of shear stress τ *vs* shear displacement δv and in terms of normal displacement δu *vs* shear displacement δv. For both methods, the results of three parametric analyses (1c, 2d, 3d) were selected to discuss the cases in which the dilatancy is more relevant. For sake of comparisons, the theoretical trend of the plastic normal displacement u_{pl} *vs* plastic shear displacement v_{pl} is shown in Fig. 16 for both the testing methods. In particular, for the calculation of u_{pl} according to Equation (7), the average compressive stress σ present on the joint after the removal of the bricks was considered; the so obtained value was doubled to account for the presence of two sliding mortar joints. The comparisons between δu *vs* δv and u_{pl} *vs* v_{pl} are considered consistent since the elastic component of the displacements became negligible once the shear failure was activated. In Tables 4 and 5, a summary of the results is presented to quantitatively evaluate the differences between the considered models in terms of peak load (P_{peak}), average shear strength (τ_{max}), average compressive stress at the peak (σ_{max}), shear displacement at the peak (δv_{peak}) and normal displacement at the peak (δu_{peak}). Percentage changes with respect to the values obtained for the reference models (A1 and B1) are included.

Concerning *Method A*, it can be observed that, for all parameters, the considered variations have a limited impact on the results in terms of shear capacity: the highest percentage variations are registered for the parametric analyses on ψ_0, but they are less than 5%. These variations can be associated to a slight compressive stress increase on the sliding interfaces. Indeed, in all cases, the normal displacements (Fig. 14b) are smaller than the theoretical ones shown in Fig. 16, indicating that they are restrained due to the test conditions. Dilatancy can therefore play a role, determining an increase in the peak load. The effect of dilatancy on the shear response is also visible by looking at the τ *vs* δv curve (Fig. 14a), where the shear crack initiation load (point in which the failure criterion is reached in all the integration points of the interfaces) and the peak load can be distinguished. In particular, the shear crack

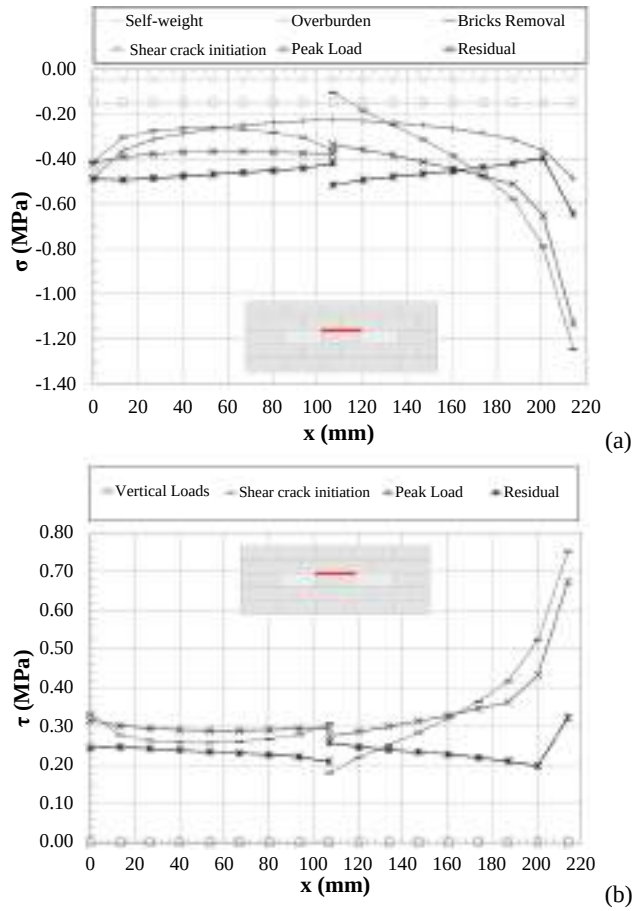

Fig. 13. Stress evolution along the top sliding interface for Model B1: (a) normal stress; (b) shear stress.

Table 3
Parametric studies on dilatancy.

Numerical simulation		ψ_0 (°)	σ_u (MPa)	δ (-)
Method *A*	**Method *B***			
A1*	B1*	21.4	−0.58	9.63
A1_1b	B1_1b	26.5	−0.58	9.63
A1_1c	B1_1c	32.1	−0.58	9.63
A1_2b	B1_2b	21.4	−0.87	9.63
A1_2c	B1_2c	21.4	−1.31	9.63
A1_2d	B1_2d	21.4	−1.96	9.63
A1_3b	B1_3b	21.4	−0.58	6.42
A1_3c	B1_3c	21.4	−0.58	4.28
A1_3d	B1_3d	21.4	−0.58	2.85

*Reference parameters, calibrated through triplet test results.

initiation load coincided with the peak of the curve for *Model A1* and it was the same in all the models. Beyond this point, the dilatant behavior of masonry, which can be relevant in the nonlinear field, determined the mentioned increase in capacity. The variations of the parameter δ for *Method A*, rather than influencing the shear response in terms of capacity, affected the trend of the nonlinear response and, in particular, the steepness of the post-peak branch: the lower its value, the less steep is the softening branch.

Concerning *Method B*, it can be observed that the shear capacity is mostly affected by variations of the parameters σ_u, with a significant increment registered for the Model B1_2d, for which normal displacements are much smaller than the theoretical ones. It is important to point out that, in correspondence of quite high values of the compressive stress σ, which is the case when performing the test with *Method B*, the

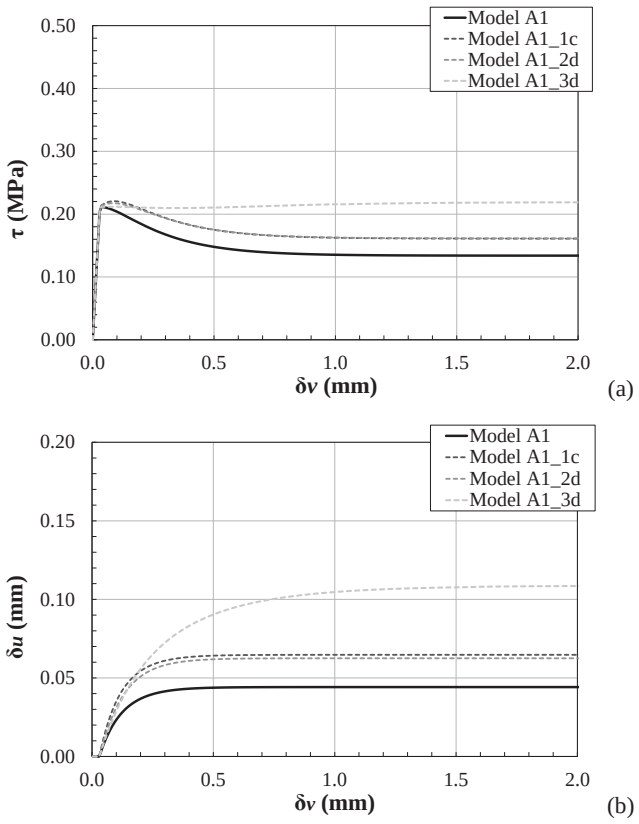

Fig. 14. Results of the parametric analyses – *Method A*: (a) shear stress τ *vs* shear displacement δ*v*; (b) normal displacement δ*u* *vs* shear displacement δ*v*.

variation in the parameter σ_u is more relevant with respect to what observed for *Method A*: the ratio σ/σ_u in Equation (8) can become the governing parameter and can have a higher effect on dilatancy. The parameter δ, as observed for *Method A*, influences the trend of the post-peak branch, without significant increases in the shear capacity, even if normal displacements are globally lower than the theoretical ones. For all the considered models, the effect of dilatancy is visible in the τ *vs* δ*v* curves, as the shear crack initiation load and the peak load do not coincide. It is worth mentioning that dilatancy could be more relevant when the shove test is performed according to *Method B* due to the boundary conditions of the test. Indeed, besides the impediment to the vertical uplift given by the surrounding masonry, already observed for *Method A*, the continuity of masonry (not disturbed by the presence of the flatjacks) can provide a greater confinement on the tested brick.

4.2. Correction factors for vertical loads

As introduced in the previous sections, the in-plane principal stress distributions and the compressive state of stress along the sliding joint could be strongly influenced, during the different phases of the shove test, by the presence of the slots for the seating of the flatjacks (*Method A* only), by the removal of the bricks, by the diffusion of the shear load, and by dilatancy. Therefore, the vertical compressive stress acting on the sliding brick is far away from being equal to the pressure applied by the flatjacks (*Method A*) or to the pressure given by the existing vertical loads (*Method B*), i.e self-weight and overburden. However, for the interpretation of the results of the test, it is very important to precisely assess the compressive stress state at failure. For *Method A*, given the reduced effect of dilatancy on the results, the actual value consists of basically two contributions: the first one is given by the vertical loads acting on the wall, namely the self-weight and the overburden, the second one is given by the flatjacks. For *Method B*, the first term only

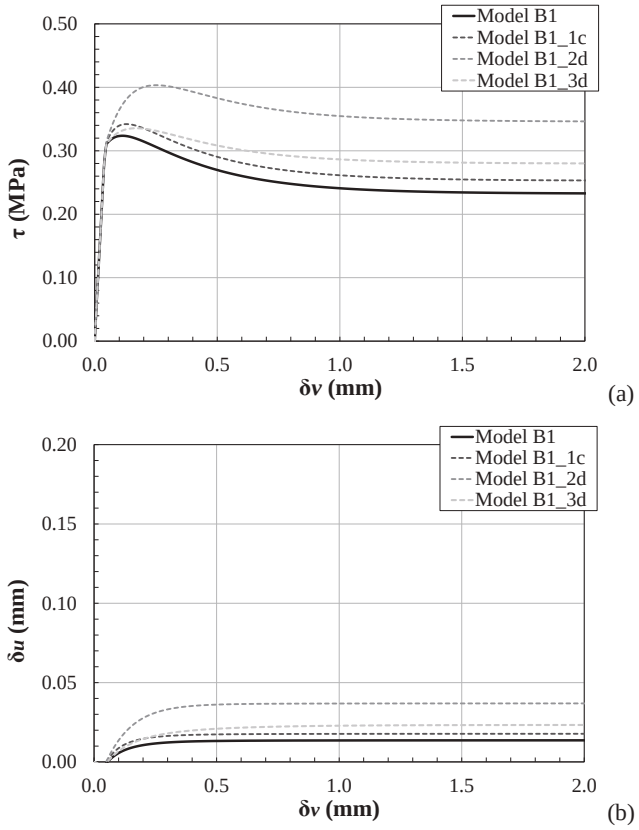

Fig. 15. Results of the parametric analyses – *Method B*: (a) shear stress τ *vs* shear displacement δv; (b) normal displacement δu *vs* shear displacement δv.

should be considered, together with a further contribution caused by dilatancy.

In order to evaluate these contributions in the practice, one possibility is to calibrate correction factors to be applied to the nominal stress values and obtained by considering the stress distributions in the different phases of the test from the numerical models. More in detail, the stress distributions were evaluated for the top and the bottom sliding joint, in each test phase (i.e. after the removal of the bricks, for both *Method A* and *B*, and after the application of the flatjack pressure, for *Method A* only), and the average compressive stress was calculated. Then, the correction factors were evaluated as the ratio between the actual average compressive stress, in the considered phases, and the nominal pressure given by the vertical loads or applied by the flatjacks (*Method A* only). These correction factors could be used in practice to estimate the actual compressive stress state on the test unit, starting from the nominal values of the applied pressure. They are additional correction factors with respect to the conversion factors introduced by the ASTM Standard C1196 [44]. Indeed, the Standard prescribes to apply conversion factors to correct the nominal flatjack pressure accounting for both the flatjack calibration procedure and the ratio of the flatjack area to the average area of the slot.

The characteristics and bond pattern of masonry surely affect the way in which vertical loads are deviated from the vertical direction, e.g. head joints not transmitting tensile stresses. Therefore, in the following, four different cases are considered for the evaluation of the above-mentioned correction factors: (i) elastic joints; (ii) no tension material for vertical and horizontal mortar joints with constant shear stiffness; (iii) no tension material for vertical and horizontal mortar joints with shear stiffness reduced by 50%; (iv) no tension material for vertical and horizontal mortar joints with zero shear stiffness.

In the present work, correction factors were calibrated for vertical loads and flatjack pressure only, given that the contribution of dilatancy

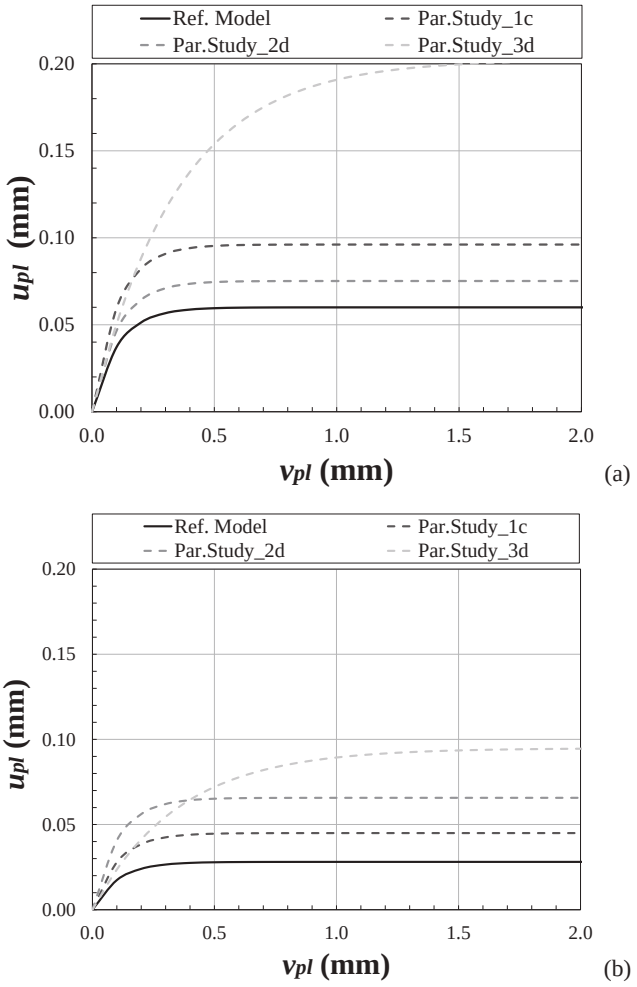

Fig. 16. Theoretical plastic normal displacement u_{pl} *vs* plastic shear displacement v_{pl}: (a) *Method A*; (b) *Method B*.

(*Method B*) became relevant beyond the point to which the sliding failure can be associated, i.e. the shear crack initiation load highlighted in the previous Sections. The obtained correction factors are reported in Table 6. As concerns *Method A*, it can be noticed how, by decreasing the shear stiffness of the joints, the correction factor for vertical load decreases, while the correction factor for the flatjack pressure increases, which is consistent with the influence that the shear stiffness has on the diffusion of the stresses inside the masonry. For *Method B*, the correction factors are basically not influenced by the changes in the shear stiffness values.

5. Validation of the model

The validation of the present model was carried out by considering a case study, part of an experimental campaign conducted at Delft University of Technology, in which the shove test was performed on a replicated single-wythe calcium silicate masonry wall, according to the *Method A* [34]. For the construction of the wall, calcium silicate bricks, having dimensions of 214 × 102 × 72 mm^3 and cementitious mortar, with joint thickness equal to 10 mm, were used.

The materials were the same adopted for the triplet test samples. The geometry and the bond pattern of the wall panel were chosen to reproduce a typical Dutch masonry wall, with one-story height. To simulate the in-situ state of stress of a typical multi-story masonry building, an overburden load was applied at the top of the wall, by pre-stressing four steel rods connected to a transverse beam, in order to

Table 4
Model A1 – Results of the parametric analyses.

Model	ψ_0	σ_u	δ	*Ppeak*	*τmax*	*σmax*	*δv,peak*	*δu,peak*
	(°)	(MPa)	(-)	(kN)	(MPa)	(MPa)	(mm)	(mm)
Model A1	21.4	−0.58	9.63	9.23	0.211	0.163	0.036	0.003
Model A1_1b	26.5	−0.58	9.63	9.36	0.214	0.171	0.060	0.017
	24.0%	(-)	(-)	1.4%	1.4%	4.9%	66.7%	529.6%
Model A1_1c	32.1	−0.58	9.63	9.63	0.221	0.181	0.087	0.030
	50.0%	(-)	(-)	4.3%	4.3%	11.2%	140.6%	1021.2%
Model A1_2b	21.4	−0.87	9.63	9.29	0.213	0.166	0.054	0.011
	(-)	50.0%	(-)	0.6%	0.6%	1.7%	48.6%	316.2%
Model A1_2c	21.4	−1.31	9.63	9.39	0.215	0.170	0.071	0.020
	(-)	125.9%	(-)	1.7%	1.7%	4.5%	97.4%	626.9%
Model A1_2d	21.4	−1.96	9.63	9.49	0.217	0.175	0.083	0.025
	(-)	237.9%	(-)	2.8%	2.8%	7.3%	129.7%	833.3%
Model A1_3b	21.4	−0.58	6.42	9.23	0.212	0.163	0.037	0.003
	(-)	(-)	−33.3%	0.0%	0.0%	0.0%	2.9%	19.8%
Model A1_3c	21.4	−0.58	4.28	9.24	0.212	0.163	0.036	0.003
	(-)	(-)	−55.6%	0.1%	0.1%	0.1%	−0.2%	1.8%
Model A1_3d	21.4	−0.58	2.85	9.56	0.219	0.178	2.420	0.109
	(-)	(-)	−70.4%	3.6%	3.6%	9.3%	6615.8%	3907.5%

Table 5
Model B1 – Results of the parametric analyses.

Model	ψ_0	σ_u	δ	*Ppeak*	*τmax*	*σmax*	*δv,peak*	*δu,peak*
	(°)	(MPa)	(-)	(kN)	(MPa)	(MPa)	(mm)	(mm)
Model B1	21.4	−0.58	9.63	14.13	0.324	0.387	0.113	0.007
Model B1_1b	26.5	−0.58	9.63	14.45	0.331	0.405	0.120	0.009
	24.0%	(-)	(-)	2.3%	2.3%	4.6%	6.1%	35.0%
Model B1_1c	32.1	−0.58	9.63	14.93	0.342	0.424	0.128	0.011
	50.0%	(-)	(-)	5.7%	5.7%	9.5%	12.8%	67.6%
Model B1_2b	21.4	−0.87	9.63	15.28	0.350	0.44	0.173	0.016
	(-)	50.0%	(-)	8.2%	8.2%	13.6%	52.6%	138.9%
Model B1_2c	21.4	−1.31	9.63	16.54	0.379	0.50	0.218	0.024
	(-)	125.9%	(-)	17.1%	17.1%	28.6%	92.8%	266.1%
Model B1_2d	21.4	−1.96	9.63	17.61	0.403	0.55	0.253	0.031
	(-)	237.9%	(-)	24.7%	24.7%	41.2%	123.7%	367.8%
Model B1_3b	21.4	−0.58	6.42	14.32	0.328	0.40	0.135	0.009
	(-)	(-)	−33.3%	1.4%	1.4%	2.3%	19.7%	36.3%
Model B1_3c	21.4	−0.58	4.28	14.50	0.332	0.40	0.152	0.011
	(-)	(-)	−55.6%	2.6%	2.6%	4.4%	34.3%	64.6%
Model B1_3d	21.4	−0.58	2.85	14.65	0.336	0.41	0.169	0.013
	(-)	(-)	−70.4%	3.7%	3.7%	6.2%	49.2%	90.6%

Table 6
Correction factors.

Model variations	Model A1		Model B1
	Vertical loads*	Flatjack pressure	Vertical loads*
Elastic joints	0.74	1.10	1.90
No tension & constant shear stiffness	0.64	1.21	1.93
No tension & reduced shear stiffness	0.63	1.21	1.93
No tension & zero shear stiffness	0.58	1.25	1.92

*Self-weight and overburden.

produce a vertical compressive stress equal to 0.25 MPa. The shove test was performed in the lower portion of the wall (Fig. 2).

The testing procedure adopted in the experimental campaign is reported in Fig. 17. Additional phases, with respect to the procedure reported in the ASTM Standard [22], were considered, according to a proposal found in previous researches [23–25], to improve the understanding of the aspects previously mentioned regarding the estimation of the compressive stress state on the sliding joints. More in detail, after the application of the overburden (*Phase 00*), the single flatjack test was performed (*Phases 01* and *02*), according to the ASTM Standard C1196-14 [44], with the aim of evaluating and verifying the compressive stress state given by the self-weight and the applied overburden. The average compressive stress σ was found to be in the range of 0.22–0.27 MPa, perfectly in line with the stress given by the applied vertical loads. The second slot was cut (*Phase 03*) to perform the double flatjack test in the initial configuration (*Phase 04*), before the removal of the bricks. The test was conducted according to the ASTM Standard C1197-14 [45] to evaluate the elastic modulus of masonry *E*. Four vertical LVDTs, with a gage length of 290 mm, were positioned to measure the displacements in this phase. The elastic modulus *E* resulted to be equal to 9975 MPa, considering all the LVDTs, and 7945 MPa, considering the central LVDTs only. Afterwards, the two bricks adjacent to the test unit and their mortar joints were accurately removed (*Phase 05*). In this phase, the LVDTs were detached from the masonry surface in order not to damage them during the extraction procedure. The double flatjack test was performed again after the removal of the bricks, in the shove test configuration (*Phase 06*), to determine a different elastic modulus *E**. This was done in order to evaluate the jack-to-brick correction factor [24] as:

$$k_{bj} = \frac{E}{E^*} = \frac{\sigma_{brick,FJ}}{\sigma_{FJ}} \tag{9}$$

where *E* is the elastic modulus evaluated with the double flatjack test in the initial configuration, *E** is the elastic modulus evaluated in the shove test configuration, $\sigma_{brick,FJ}$ is the actual vertical compressive stress

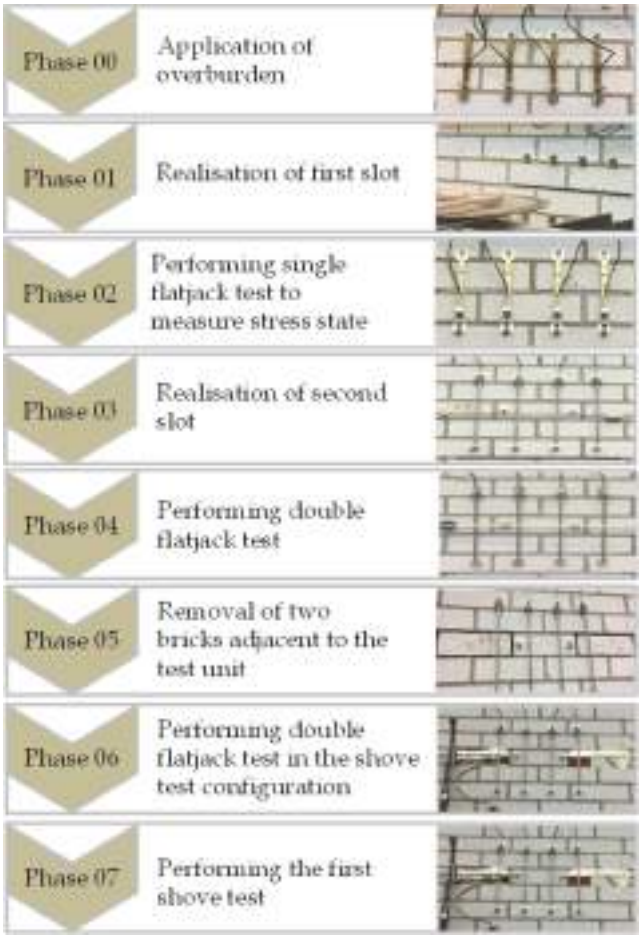

Fig. 17. Shove Test – *Method A*: testing procedure [34].

on the test unit due to the flatjack pressure, σ_{FJ} is the pressure applied by the flatjacks, evaluated using the conversion factors prescribed by the ASTM Standard C1196 [44], accounting for both the flatjack calibration procedure and the ratio of the flatjack area to the average area of the slot. The elastic modulus E^* was evaluated by considering the two central LVDTs only and it was equal to 6750 MPa. Therefore, the value of the jack-to-brick correction factor k_{bj} resulted to be equal to 1.18. Due to its definition, it can be directly compared with the values of the correction factors obtained through the numerical analyses for the flatjack pressure of Model A1 (Table 6). A very good agreement can be noticed.

The setup of the shove test (*Phase 07*) is presented in Fig. 17. During the test, horizontal and vertical displacements were measured by means of LVDTs: two horizontal LVDTs were positioned on both sides of the test unit to measure its relative displacement with respect to the surrounding masonry, and two vertical LVDTs were positioned in correspondence of the test unit to monitor the displacements orthogonal to the mortar joint (dilatancy) during the sliding failure. Moreover, LVDTs were placed at the wall sides to check undesired failure modes, e.g. failure of the masonry portion behind the horizontal jack. At the beginning of the test, the pressure in the two flatjacks was set at a low value ($\sigma_1 = 0.065$ MPa) and the shear force was applied monotonically by means of the horizontal jack. After attaining the first sliding, the pressure in the flatjacks was increased four more times and the brick was further slid a corresponding number of times. The failure mode was characterized by the sliding of the test unit along the brick-mortar interfaces, and it did not involve bricks, thus supporting the modeling hypothesis described in Section 2.1.

The results of the shove test, at each load step, are reported in Table 7, where: τ is the maximum shear stress (only for the first step it is necessary to distinguish between the peak shear strength and the residual one), σ_{FJ} is the flatjack pressure, $\sigma_{brick,FJ}$ is the vertical compressive stress on the test unit due to the flatjack pressure, evaluated as $\sigma_{FJ}{}^*k_{bj}$ (Equation (9)), $\sigma_{brick,OB}$ is the vertical compressive stress on the test unit due to the overburden, evaluated by multiplying the overburden stress and the correction factor for vertical loads (equal to 0.64) reported in Table 6, and σ_{real} is the compressive stress on the test unit given by the sum of $\sigma_{brick,FJ}$ and $\sigma_{brick,OB}$. It is worth mentioning that since the LVDTs were detached during the removal of the bricks (*Phase 05*), it was not possible, in this case, to experimentally evaluate the correction factor for vertical loads. Given the good agreement found between the numerical and experimental findings for what concerns the correction factor k_{bj}, it seemed consistent here to use the correction factor for vertical loads found from the numerical analyses, considered equal to 0.64.

Table 7
Case study – Shove test results.

Load Step	σ_{FJ} (MPa)	$\sigma_{brick,FJ}$ (MPa)	$\sigma_{brick,OB}$ (MPa)	σ_{real} (MPa)	τ (MPa)
Load Step 1 - Peak	0.065	0.076	0,160	0.236	0.292
Load Step 1	0.065	0.076	0,160	0.236	0.087
Load Step 2	0.140	0.164	0,160	0.324	0.171
Load Step 3	0.272	0.320	0,160	0.480	0.256
Load Step 4	0.427	0.503	0,160	0.663	0.389
Load Step 5	0.565	0.665	0,160	0.825	0.398

The failure points obtained can be reported in a σ - τ diagram for the evaluation of the residual Coulomb friction failure criterion. From the diagram in Fig. 18a, where the failure points were plotted by considering $\sigma_{brick,FJ}$ as the acting compressive stress on the test unit, it is possible to notice that the residual Coulomb friction failure criterion is not characterized, as it should be, by a zero cohesion. This can be explained by considering that these values of the compressive stresses were not corrected by introducing the contribution of the vertical loads. A proper evaluation of the actual compressive stress on the test unit was here obtained by using the correction factor for vertical loads found in the numerical models. It can be seen that, by plotting the obtained (σ_{real};τ) points in the diagram (Fig. 18b), an almost null cohesion was obtained. The value of the friction coefficient was 0.55, which is quite close to the value found in the experimental campaign on triplet tests (equal to 0.50). The friction coefficient is the same in both cases since, as can be seen in the second graph, the points are simply translated to the right by the same quantity. With the execution of a single shove test, only one initial failure point is available. Therefore, an estimation of the cohesion cannot be provided.

It is worth pointing out that, with the corrections considered for the compressive stress values, it is tacitly assumed that dilatancy is not affecting the results in terms of capacity, as was found in the results for Model A1. Therefore, in this case, an increase in the compressive stress on the sliding brick is not expected due to dilatancy. This is consistent with the experimental behavior, in which shear crack initiation load and peak load, as previously defined, coincided (Fig. 19).

In Fig. 19a and b, the experimental shear stress τ *vs* shear displacement δv and the normal displacement δu *vs* shear displacement δv curves are reported, respectively. The experimental post-peak dashed line in Fig. 19a has a straight pattern since it connects the peak with one single point, highlighting the fact that the post-peak phase could not be correctly controlled and identified. The experimental test was indeed performed under force control. The results of the numerical simulations for load steps 1 to 4 are reported as well to compare the results and validate the model. In particular, in Fig. 19b, only the first load step is considered, given that dilatancy is effective for low values of the plastic shear displacements, according to its definition. With reference to Fig. 19a, it is possible to notice that, in the first load step, a lower peak stress and a higher residual stress were obtained in the numerical

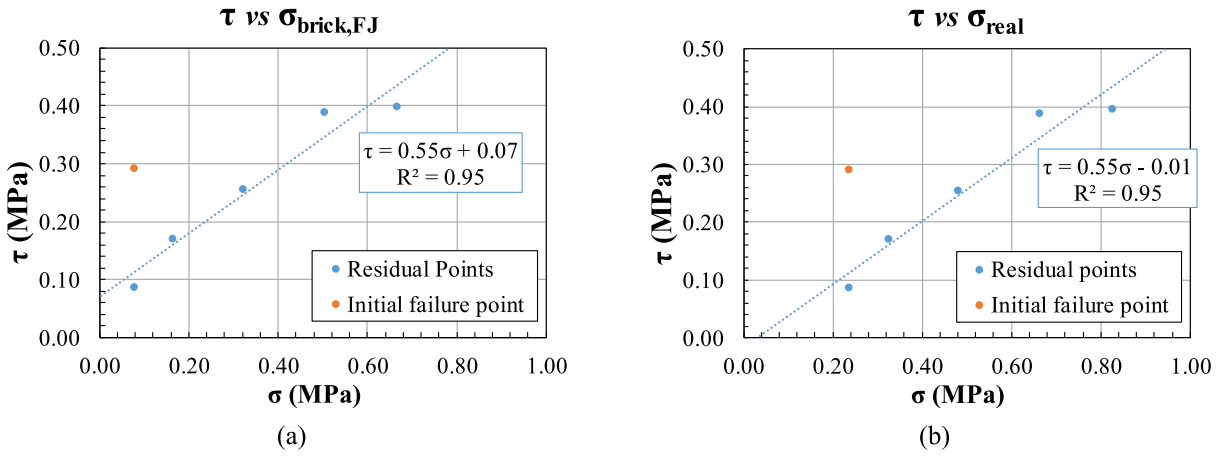

Fig. 18. Case study – Shove test results: σ-τ diagrams.

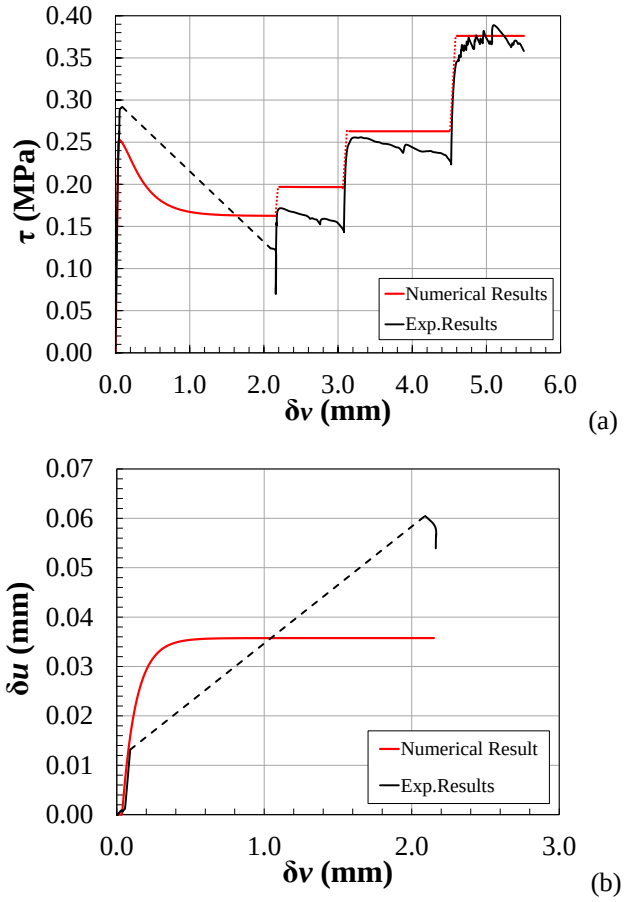

Fig. 19. Case study – Shove test: experimental *vs* numerical results: (a) shear stress τ *vs* shear displacement δ*v*; (b) normal displacement δ*u* *vs* shear displacement δ*v*.

analysis with respect to the experimental results. A slight difference in the failure criteria calibrated from triplet test and shove test results, in correspondence of a low compressive stress, can determine these discrepancies. In the following load steps, instead, a better agreement was found, especially in the third and fourth load steps. A very good agreement can be noticed in the first part of the graph of Fig. 19b. However, in correspondence of the reaching of the peak load, the experimental normal displacements are much higher than the ones obtained with the numerical analysis. This can be related to the fact that, during the experimental tests, rigid movements of the sliding brick (e.g. rotation) influenced the final value of the normal displacements. Worth mentioning that their absolute value is small and thus sensitive even to limited experimental anomalies. Despite this, the numerical model seems to be capable of reproducing the shear-sliding failure mode observed experimentally in the shove test and, moreover, reliable estimation of the actual compressive state of stress helped in the interpretation of the results and in the calibration of the residual Coulomb friction failure criterion.

6. Discussions

The objective of this Section is to discuss the findings of the numerical analyses and provide some useful indications for the common practice, in which the considered experimental tests are applied to existing structures. To this purpose, comparisons between *Method A* and *Method B* of the shove test and between shove test and triplet test will be discussed.

6.1. Shove test – Method A vs Method B

In the shove test, a single test unit is displaced horizontally with respect to the surrounding masonry by means of a horizontal hydraulic jack. The test unit is also subject to a vertical load, either applied by flatjacks positioned above and below the test unit (*Method* A) or estimated from the acting dead and live loads (*Method B*). Due to the presence of the flatjacks, in *Method A*, it is possible to perform the test more than once at a single location, by varying the compressive stress via the flatjacks.

The main advantages of *Method A* with respect to *Method B* are: the possibility to perform, prior to the shove test, single and double flatjack tests on the tested masonry portion, thus obtaining an estimation of the acting vertical loads and of the deformability properties of masonry, and the possibility to execute the shove test at different vertical compression stress levels. This is useful to obtain an accurate estimation of the residual Coulomb friction criterion from one single test. However, in order to calibrate the initial failure criterion, without making any assumption on the friction coefficient, the execution of more than one test is needed. If possible, at least three tests on the same masonry typology should be performed. The drawbacks of *Method A* are the complexity of the test itself and the great uncertainties involved in the definition of the wall in-plane stress distribution and, more specifically, of the vertical compressive stress acting on the sliding brick, due to the effects of the execution of the flatjack slots and of the removal of the lateral bricks. In practice, it is quite difficult to correctly evaluate these contributions, since they substantially depend on the ability of the masonry of transferring loads, which can be extremely variable in existing, and maybe

damaged or deteriorated, masonries. Moreover, it was observed from numerical analyses that, for very low value of flatjack pressure, the vertical compressive stress state on the considered brick is mainly provided by the overburden load than by the flatjack. Therefore, if a correct evaluation of the overburden contribution to the vertical compressive stress state is not carried out, the results, in terms of vertical stress at failure, can lead to the calibration of an incorrect failure domain. Furthermore, when dilatancy is relevant for the shear-sliding response of masonry, which was not the case for the calcium silicate brick masonry here considered, the problem could become even more complex.

The main advantage of *Method B* is the greater simplicity and quick execution with respect to *Method A*, which is surely an aspect to be taken into account when planning an experimental campaign on existing constructions. Moreover, a lower disturbance is created to the wall panel since the cuts for the seating of the flatjacks are not executed. To obtain information on the compressive state of stress of the wall prior to testing, single and double flatjack tests could be performed on the same masonry, close to the tested portion. In this way, less uncertainties will be related to the estimation of the compressive stress on the test unit. However, for *Method B*, more than one test have to be executed on the same masonry typology to calibrate both the residual and the initial Coulomb friction failure criterion.

Comparing the results of Models A1 and B1, performed by considering the same overburden load, it is evident that the shear capacity is greater in the latter case, due to the fact that a higher vertical compressive stress state is present. Also, due to test conditions, vertical uplifts upon shearing are more restrained for Model B1, and this can determine a greater impact of dilatancy on the shear capacity of masonry. From the presented numerical simulations, the diffusion of the shear load seems to have a greater influence on the compressive stress when performing the test with *Method B*. However, this latter observation could be also related to the features of the masonry here considered (small dilatancy value) and may not be generalized for different masonry typologies, e.g. clay brick masonry.

As evidenced throughout the paper, one of the most important aspects, when performing a shove test, is the correct estimation of the vertical compressive stress state on the test unit. To this purpose, correction factors were introduced and calibrated to evaluate the contribution given by the flatjack pressure (*Method A* only) and by the vertical loads. In this way, in the engineering practice, by multiplying the correction factors and the correspondent nominal values of the applied pressures, given by the flatjacks (*Method A* only) or by the vertical loads, the compressive stress acting on the sliding joint, at the beginning of the test, can be correctly evaluated. The correction factors can be calibrated through numerical analyses, considering different masonry typologies and specific geometries and test setups. Alternatively, they can be evaluated during the execution of the shove test.

To improve the testing procedure, for both methods, it is suggested to position vertical LVDTs in correspondence of the test unit. On the one hand, they can be useful to monitor the displacements during the removal of the bricks, in order to evaluate the average compressive stress increase in the tested masonry portion, given that the elastic properties of the masonry in the shove test configuration can be determined as previously described [24]. In this way, it is possible to evaluate the correction factor for vertical loads. On the other hand, the presence of vertical LVDTs can be of great help in the detection of a dilatant behavior of masonry. To calibrate the Coulomb friction failure criterion, indeed, it is important to detect the shear crack initiation load rather than the peak load. The peak shear strength, if different from that at shear crack initiation, is associated to an increase in the compressive stress due to dilatancy and should not be confused with the actual shear strength of the material. Using vertical LVDTs, the shear crack initiation load can be identified as the point from which positive vertical displacements are observed.

6.2. Shove test vs triplet test

Triplet tests are performed on small masonry samples and allow to identify the mechanical properties of masonry according to a Coulomb friction failure criterion. Since they are performed in laboratory, displacement-controlled procedures may be used, even if requiring quite complex setup, and the post-peak phase can be characterized as well. This is very useful to obtain accurate input parameters to be used in the numerical simulations. On the contrary, with the shove test, which is executed under force control, the identification of the post-peak phase is more difficult and cannot be properly achieved. Even if the testing procedures are different, i.e. force or displacement control, similar results in terms of calibrated failure criteria would be expected. However, differences can be observed both in the test setup and in the conditions of the samples, leading to different test outcomes.

First of all, the boundary conditions are not the same and they influence the stress distributions along the sliding joints. Being the uniformity of compressive and shear stresses one of the most important features of a shear test [46], it is evident that this aspect can determine discrepancies between the triplet and the shove test results. Secondly, triplet tests are very small samples compared to the wall panels considered for the shove tests. Even if the presence of head joints is included in the triplet test specimens (i.e. modified triplet test), thus considering the same bond pattern of the shove test, the construction process of the triplet samples and their curing conditions (e.g. vertical loads to which they are subjected) are very different from the ones of the walls used for the shove test.

Finally, the compressive stress state along the joints can be very different in the two tests. In the shove test, it is not simply the applied one, but it is influenced by many contributions, as previously described. On the other hand, in the triplet test, the displacement orthogonal to the sliding joint can be considered free while in the shove test it is more restrained, due to the test conditions already discussed. Therefore, in the shove test, dilatancy could determine a further increase in compressive stress, while in the triplet test, dilatancy is only recognizable in terms of normal displacements registered along the joints during the sliding failure. It has been demonstrated in this paper that, if a correct estimation of the compressive stress state in the shove test is carried out, the differences between the outcomes of the shove test and the triplet test can be significantly reduced.

7. Conclusions

In the present paper, a numerical study on the use of the shove test to investigate the shear-sliding behavior of masonry was presented. Nonlinear numerical analyses were performed considering two testing methods: *Method A* and *B*, as defined in the ASTM Standard C1531 [22]. The main difference between *Method A* and *Method B* is the way in which the vertical compression is controlled or evaluated during the test: in *Method A* flatjacks are positioned above and below the test unit and the tested masonry portion is directly loaded in compression; in *Method B*, the compressive stress state is evaluated through load analyses. After the removal of the bricks adjacent to the test unit, in both testing methods, a horizontal force is applied by means of a hydraulic jack to produce the sliding of the test unit with respect to the surrounding masonry. Differently than *Method B*, for *Method A* multiple tests can be performed in the same location by varying the vertical compressive stress via the flatjacks.

A brick-to-brick modeling approach was adopted and the combined cracking-shearing-crushing model, including a tension cut-off, a Coulomb friction criterion and a compressive cap, was assigned to the zero-thickness interface elements modeling the sliding mortar joints. The nonlinear model was calibrated by considering the results of triplet tests performed on standard specimens, arranged with a stacked bond, and on modified specimens, built with a running bond pattern, to include the presence of head joints. The model was then validated by

comparison with the results of an experimental campaign, in which a shove test was performed on a calcium silicate masonry wall, according to *Method A*. Parametric studies were also performed to study how dilatancy can affect the results of the shove test, both in terms of shear behavior and peak shear strength.

After having highlighted the main advantages and disadvantages of the two testing methods, the results of the numerical analyses allowed to understand which aspects could most affect the shear-sliding behavior of masonry and to draw the following conclusions:

- The boundary conditions of the tests have a great impact on the test results, especially on the vertical compressive stress state on the sliding brick, which can be different from the one applied by the flatjacks (*Method A*) or from the one estimated by the acting dead and live loads (*Method B*). The vertical compressive stress is influenced by the presence of the slots for the seating of the flatjacks (*Method A* only), by the removal of bricks, by the diffusion of the shear load and by dilatancy.
- To correctly evaluate the compressive stress state, correction factors for vertical loads and for flatjack pressure were calibrated for the investigated masonry typology. Given that dilatancy did not influence to a great extent the experimental results in terms of capacity, the evaluation of the contributions of the flatjack pressure and of the vertical loads was here considered sufficient.
- A proposal for the modification of the test procedure and setup was made, i.e. including vertical additional LVDTs, to be positioned in correspondence of the test unit. They can be useful to monitor the displacements during the removal of the bricks, allowing for the experimental evaluation of the correction factor for vertical loads. In addition, they can help in the detection of a dilatant behavior of masonry and in the identification of the shear crack initiation load.
- If the correct failure state of stress is identified in the shove test, using the proposed correction factors, a good correspondence between the results of shove tests and triplet test can be found.

CRediT authorship contribution statement

F. Ferretti: Conceptualization, Methodology, Data curation, Formal analysis, Investigation, Validation, Writing – original draft, Writing – review & editing. **S. Jafari:** Data curation, Resources, Formal analysis, Investigation, Writing – review & editing. **R. Esposito:** Project administration, Conceptualization, Resources, Validation, Writing – review & editing. **J.G. Rots:** Funding acquisition, Project administration, Conceptualization, Writing – review & editing. **C. Mazzotti :** Conceptualization, Validation, Writing – review & editing.

Declaration of Competing Interest

The authors declare that they have no known competing financial interests or personal relationships that could have appeared to influence the work reported in this paper.

Acknowledgements

The experimental tests reported in this paper were funded by Nederlandse Aardolie Maatschappij (NAM), under contract number UI63654 “Testing program 2016 for Structural Upgrading of URM Structures” (contract holders Dick den Hertog and Reza Sarkhosh), which is gratefully acknowledged. The first author would like to acknowledge the “Marco Polo” mobility program of the University of Bologna, that provided funding for her visiting period at Delft University of Technology.

References

[1] Anthoine A. In-plane behaviour of masonry: a literature review; 1992. Available from: https://op.europa.eu/en/publication-detail/-/publication/0da3569f-7626-4c9a-b140-666d2d9c05ba.
[2] Magenes G, Calvi GM. In-plane seismic response of brick masonry walls. Earthq Eng Struct Dyn 1997;26:1091–1112. doi: 10.1002/(SICI)1096-9845(199711)26:11<1091::AID-EQE693>3.0.CO;2-6.
[3] Tomaževič M. Shear resistance of masonry walls and Eurocode 6: shear versus tensile strength of masonry. Mater Struct 2009;42(7):889–907. https://doi.org/10.1617/s11527-008-9430-6.
[4] Calderini C, Cattari S, Lagomarsino S. In-plane strength of unreinforced masonry piers. Earthq Eng Struct Dyn 2009;38(2):243–67. https://doi.org/10.1002/eqe.860.
[5] Messali F, Esposito R, Ravenshorst GJP, Rots JG. Experimental investigation of the in-plane cyclic behaviour of calcium silicate brick masonry walls. Bull Earthq Eng 2020;18(8):3963–94. https://doi.org/10.1007/s10518-020-00835-x.
[6] Mann W, Muller H. Failure of shear-stressed masonry - an enlarged theory, tests and application to shear walls. In: Proc. int. syposium load bear. Brickwork, London; 1980.
[7] Calderini C, Cattari S, Lagomarsino S. The use of the diagonal compression test to identify the shear mechanical parameters of masonry. Constr Build Mater 2010;24(5):677–85. https://doi.org/10.1016/j.conbuildmat.2009.11.001.
[8] Penna A, Morandi P, Rota M, Manzini CF, da Porto F, Magenes G, et al. earthquake. Bull Earthq Eng 2012;12(2014):2255–73. https://doi.org/10.1007/s10518-013-9496-6.
[9] Ferretti F, Ferracuti B, Mazzotti C, Savoia M. Destructive and minor destructive tests on masonry buildings: experimental results and comparison between shear failure criteria. Constr Build Mater 2019;199:12–29. https://doi.org/10.1016/j.conbuildmat.2018.11.246.
[10] Van der Pluijm R, Rutten H, Ceelen M. Shear behavior of bed joints. In: 12th int. brick block mason. conf., Madrid; 2000.
[11] Schubert P, Glitza H. Festigkeits un Verformungswerte von Mauermörtel und Wandbausteinen; 1978.
[12] Drysdale RG, Vanderkeyl R, Hamid AA. Shear strength of brick masonry joints. In: Proc. 5th int. brick block mason. conf., Washington D.C.; 1979.
[13] Stöckl S, Hofmann P, Mainz J. A comparative finite element evaluation of mortar joint shear tests. Mason Int 1990;3:101–4.
[14] Riddington JR, Jukes P. A masonry joint shear strength test method. In: Proc. instn civ. engrs structs bldgs, vol. 104; 1994. p. 267–74.
[15] Van der Pluijm R. Material properties of masonry and its components under tension and shear. In: Proc. 6th Can. mason. symp., Saskatoon, Canada; 1992. p. 675–86.
[16] Popal R, Lissel SL. Numerical evaluation of existing mortar joint shear tests and a new test method. In: proc. 8th int. mason. conf., Dresden; 2010.
[17] EN 1052-3. Methods of test for masonry - Part 3: Determination of initial shear strength; 2002.
[18] Vermeltfoort AT. Variation in shear properties of masonry. International Masonry Society; 2010. p. 159–68.
[19] Zhang S, Richart N, Beyer K. Numerical evaluation of test setups for determining the shear strength of masonry. Mater Struct 2018;51:110. https://doi.org/10.1617/s11527-018-1236-6.
[20] Atkinson RH, Kingsley GR, Sture S. A laboratory and in situ study of the shear strength of masonry bed joints. In: Proc. 8th int. brick/block mason. conf.; 1988. p. 261–71.
[21] Noland JL, Kingsley GR, Atkinson RH. Utilization of nondestructive techniques into the evaluation of masonry. In: Proc. 8th int. brick/block mason. conf.; 1988.
[22] ASTM C1531-16. Standard test methods for in situ measurement of masonry mortar joint shear strength index; 2016.
[23] Andreotti G, Graziotti F, Magenes G. Detailed micro-modelling of the direct shear tests of brick masonry specimens: the role of dilatancy. Eng Struct 2018;168:929–49. https://doi.org/10.1016/j.engstruct.2018.05.019.
[24] Graziotti F, Guerrini G, Rossi A, Andreotti G, Magenes G. Proposal for an improved procedure and interpretation of ASTM C1531 for the in situ determination of brick-masonry shear strength. In: Mason. 2018, ASTM International, 100 Barr Harbor Drive, PO Box C700, West Conshohocken, PA 19428-2959; 2018. p. 13–33. doi: 10.1520/STP161220170181.
[25] Andreotti G, Graziotti F, Magenes G. Expansion of mortar joints in direct shear tests of masonry samples: implications on shear strength and experimental characterization of dilatancy. Mater Struct 2019;52:64. https://doi.org/10.1617/s11527-019-1366-5.
[26] Rots JG. Structural masonry: an experimental/numerical basis for practical design rules. Balkema, Rotterdam; 1997.
[27] van Zijl GPAG. Modeling masonry shear-compression: role of dilatancy highlighted. J Eng Mech 2004;130(11):1289–96. https://doi.org/10.1061/(ASCE)0733-9399(2004)130:11(1289).
[28] Bonura V, Jafari S, Zapico Blanco B, Graziotti F. Interpretation of in situ shear test for brick masonry: a benchmark study. In: Proc. 16th Eur. conf. earthq. eng. 16ECEE; 2018. p. 18–21.
[29] Lourenço PB, Rots JG, Blaauwendraad J. Two approaches for the analysis of masonry structures - micro and macro-modeling. Heron 1995;40:313–40.
[30] Lourenço PB. Computational strategies for masonry structures. Delft University of Technology; 1996.
[31] Roca P, Cervera M, Gariup G, Pela’ L. Structural analysis of masonry historical constructions. Classical and advanced approaches. Arch Comput Methods Eng 2010;17:299–325. https://doi.org/10.1007/s11831-010-9046-1.

[32] Angelillo M, Lourenço PB, Milani G. Masonry behaviour and modelling. In: CISM int. cent. mech. sci. courses lect.; 2014. p. 1–26. doi: 10.1007/978-3-7091-1774-3_1.
[33] D'Altri AM, Sarhosis V, Milani G, Rots J, Cattari S, Lagomarsino S, et al. A review of numerical models for masonry structures. In: Numer. model. mason. hist. struct. Elsevier; 2019. p. 3–53. doi: 10.1016/B978-0-08-102439-3.00001-4.
[34] Jafari S, Ferretti F, Esposito R. Flatjack and shove tests: method validation and correlation; 2018. Available from: https://research.tudelft.nl/en/publications/flatjack-and-shove-tests-method-validation-and-correlation-c31b67.
[35] Jafari S, Esposito R. Material tests for the characterisation of replicated calcium silicate brick masonry. Delft University of Technology; 2016. Available from: https://research.tudelft.nl/en/publications/material-tests-for-the-characterisation-of-replicated-calcium-sil.
[36] Lourenço PB, Rots JG. Multisurface interface model for analysis of masonry structures. J Eng Mech 1997;123(7):660–8. https://doi.org/10.1061/(ASCE)0733-9399(1997)123:7(660).
[37] Jafari S, Rots JG, Esposito R. Core testing method to assess nonlinear shear-sliding behaviour of brick-mortar interfaces: a comparative experimental study. Constr Build Mater 2020;244:118236. https://doi.org/10.1016/j.conbuildmat.2020.118236.
[38] Vermeer PA, de Borst R. Non-associated plasticity for soils, concrete and rock. Heron 1984;29:3–64.
[39] Giambanco G, Rizzo S, Spallino R. Numerical analysis of masonry structures via interface models. Comput Methods Appl Mech Eng 2001;190(49-50):6493–511. https://doi.org/10.1016/S0045-7825(01)00225-0.
[40] Jafari S, Esposito R. Material tests for the characterization of replicated calcium silicate brick masonry - Report number C31B67WP1-9. Available from: https://research.tudelft.nl/files/83127770/Material_properties_of_CS_masonry_C31B67WP1_9_.pdf. Delft University of Technology; 2017.
[41] EN 772-1. Methods of test for masonry units - Part 1: Determination of compressive strength; 2011.
[42] EN 1052-1. Methods of test for masonry - Part 1: Determination of compressive strength; 1998.
[43] Ferretti F, Mazzotti C, Esposito R, Rots JG. Shear-sliding behavior of masonry: Numerical micro-modeling of triplet tests. In: Comput. model. concr. struct. CRC Press; 2018. p. 941–51. doi: 10.1201/9781315182964-109.
[44] ASTM C1196-14a. Standard test method for in situ compressive stress within solid unit masonry. Am Soc Test Mater 2014.
[45] ASTM C1197–14. Standard test method for in situ measurement of masonry deformability properties using the Flatjack method. Am Soc Test Mater 2014.
[46] Riddington JR, Fong KH, Jukes P. Numerical study of failure initiation in different joint shear tests. Mason Int 1997;11.